Monthly Notices of the ROYAL ASTRONOMICAL SOCIETY

MNRAS **525,** 5328–5352 (2023) https://doi.org/10.1093/mnras/stad2553
Advance Access publication 2023 August 25

On the observability and identification of Population III galaxies with *JWST*

James A. A. Trussler [1]★ Christopher J. Conselice,[1] Nathan J. Adams [1] Roberto Maiolino,[2,3,4] Kimihiko Nakajima [5] Erik Zackrisson [6] Duncan Austin [1] Leonardo Ferreira[7] and Tom Harvey [1]

[1]*Jodrell Bank Centre for Astrophysics, University of Manchester, Oxford Road, Manchester M13 9PL, UK*
[2]*Cavendish Laboratory, University of Cambridge, 19 J.J. Thomson Avenue, Cambridge CB3 0HE, UK*
[3]*Kavli Institute for Cosmology, University of Cambridge, Madingley Road, Cambridge CB3 0HA, UK*
[4]*Department of Physics and Astronomy, University College London, Gower Street, London WC1E 6BT, UK*
[5]*National Astronomical Observatory of Japan, 2-21-1 Osawa, Mitaka, Tokyo 181-8588, Japan*
[6]*Observational Astrophysics, Department of Physics and Astronomy, Uppsala University, Box 516, SE-751 20 Uppsala, Sweden*
[7]*Department of Physics & Astronomy, University of Victoria, Finnerty Road, Victoria, British Columbia, V8P 1A1, Canada*

Accepted 2023 July 31. Received 2023 July 31; in original form 2023 January 10

ABSTRACT

We utilize theoretical models of Population III stellar + nebular spectra to investigate the prospects of observing and accurately identifying Population III galaxies with *JWST* using both deep imaging and spectroscopy. We investigate a series of different colour cuts, finding that a combination of NIRCam and MIRI photometry through the *F444W*−*F560W*, *F560W*−*F770W* colours offers the most robust identifier of potential $z = 8$ Pop III candidates. We calculate that NIRCam will have to reach ∼28.5–30.0 AB mag depths (1–20 h), and MIRI *F560W* must reach ∼27.5–29.0 AB mag depths (10–100 h) to achieve 5σ continuum detections of $M_* = 10^6\,\mathrm{M}_\odot$ Pop III galaxies at $z = 8$. We also discuss the prospects of identifying Pop III candidates through slitless and NIRSpec spectroscopic surveys that target Lyα, Hβ, and/or He II λ1640. We find small differences in the Hβ rest-frame equivalent width (EW) between Pop III and non-Pop III galaxies, rendering this diagnostic likely impractical. Instead, we find that the detection of high EW He II λ1640 emission will serve as the definitive Pop III identifier, requiring (ultra-)deep integrations (5–150 h) with NIRSpec/G140M for $M_* = 10^6\,\mathrm{M}_\odot$ Pop III galaxies at $z = 8$. However, MIRI *F770W* detections of Pop III galaxies will require substantial gravitational lensing ($\mu = 10$) and/or fortuitous imaging of exceptionally massive ($M_* = 10^7\,\mathrm{M}_\odot$) Pop III galaxies. Thus, NIRCam medium-band imaging surveys that can search for high EW He II λ1640 emitters in photometry may perhaps be a viable alternative for finding Pop III candidates.

Key words: stars: Population III – galaxies: abundances – galaxies: evolution – galaxies: formation – galaxies: high-redshift.

1 INTRODUCTION

The recently launched and now fully operational *JWST* is set to usher in a golden era of astronomy, being the central catalyst for a great new age of discovery. Indeed, our perception of the Universe will forever change, as we begin to see it with a clarity and depth that greatly surpasses anything that has come before. Among its many grand discoveries set to come, perhaps the greatest of all is the possibility of observing the light from the very first stars in the Universe (e.g. Bromm & Larson 2004; Bromm & Yoshida 2011). These chemically pristine, so-called 'Population III' stars, formed out of the primordial hydrogen and helium (and trace amounts of lithium), and were the first embers to ignite, producers of the starlight that ended the cosmic dark ages (e.g. Miralda-Escudé 2003) and paved the way for cosmic dawn (e.g. Laporte et al. 2021). In studying these first stars, the foundation upon which all of cosmic history stands, we will gain unprecedented insights into both primordial star formation (e.g. Johnson 2013), as well as the characteristics of the 'Population III galaxies' within which the first stars reside (e.g. Bromm & Yoshida 2011). Indeed, by analysing Pop III galaxies, we will be witnesses to the synthesis of the very first non-primordial elements and the subsequent chemical enrichment of the Universe (e.g. Ferrara, Pettini & Shchekinov 2000; Madau, Ferrara & Rees 2001; Bromm, Yoshida & Hernquist 2003).

Forming in so-called 'atomic cooling haloes', where hydrogen gas is sufficiently hot to collisionally ionize, and thus cool through recombination, Pop III galaxies are expected, from virial arguments, to have halo masses of $M_\mathrm{h} \sim 10^8\,\mathrm{M}_\odot$ (see e.g. Johnson, Greif & Bromm 2008; Bromm & Yoshida 2011). Accounting for the cosmic baryon fraction and approximate estimates for the efficiency with which primordial baryonic gas is converted into stars, these first galaxies are believed to have a typical stellar mass of $M_* \sim 10^5\,\mathrm{M}_\odot$ (Bromm & Yoshida 2011). Thus, the combination of their low stellar masses, together with their great cosmological distances from us, makes such Pop III galaxies exceptionally faint, and therefore beyond the detection capabilities of the telescopes that came before *JWST*.

JWST, with its exceptional sensitivity and resolution, is thus the ideal facility with which to search for these elusive Pop III galaxies (e.g. Gardner et al. 2006; Bromm & Yoshida 2011; Nakajima &

★ E-mail: james.trussler@manchester.ac.uk

Maiolino 2022; Katz et al. 2023). Its extensive suite of scientific instruments and diverse observing modes, spanning imaging to both slit and slitless spectroscopy, will all play an essential role in identifying Pop III candidates and further characterizing their properties. The signatures of Pop III stars are encoded within their rest-UV-optical-NIR light. *JWST*, spanning the NIR-to-MIR wavelengths to which these fingerprints of primordial star formation are redshifted therefore has the capabilities to capture the full wealth of information stored within this ancient starlight.

The photometric and spectroscopic signatures of Pop III stars and galaxies have been extensively studied. For example, Schaerer (2002) presented realistic models for massive Pop III stars, including nebular continuum emission, finding that nebular line and continuum emission strongly affect the broad-band photometric properties of Pop III objects. Indeed, strong (i.e. high EW) emission in the He II λ1640 recombination line was found (e.g. Schaerer 2002, 2003; Raiter, Schaerer & Fosbury 2010) to be a clear signature of chemically-pristine Pop III stars, reflecting their exceptional capability in generating hard ionizing photons capable of doubly ionizing helium. This in turn is due to the likely very massive nature of Pop III stars ($\gtrapprox$10 $M_\odot$, see e.g. Bromm, Coppi & Larson 1999; Tan & McKee 2004), being the net result of inefficient cooling and subsequent star formation in metal-free, primordial gas.

Later works, such as Zackrisson et al. (2011), built upon these earlier models to generate forecasts for the prospects of *JWST* at observing and identifying Pop III galaxies. They concluded that ultra-deep exposures would be needed to detect $\sim$$10^5$ $M_\odot$ Pop III galaxies at $z = 10$, with colour–colour selections combining *JWST*/NIRCam and *JWST*/MIRI photometry enabling a clean selection of Pop III galaxies at $z \approx 7$–8. Indeed, fortuitous gravitational lensing of Pop III galaxies will greatly relax the otherwise demanding integration times needed (Zackrisson et al. 2012). At the same time, wide-field surveys with e.g. *Euclid* and the *Roman Space Telescope* (*RST*) will likely play a crucial role in our photometric search for Pop III galaxies (Vikaeus et al. 2022).

Follow-up spectroscopy, aiming to target bright emission lines such as Hβ and He II λ1640, will be essential to verify the pristine nature of potential Pop III candidates. The application of spectroscopic diagnostics, such as the He II λ4686/Hβ line ratio, will enable us to distinguish between different types of chemically pristine and extremely metal-poor systems (Nakajima & Maiolino 2022). In this regard, *JWST*, but also the next-generation of extremely large telescopes, will play a pivotal role in definitively identifying true Pop III galaxies (Grisdale et al. 2021; Nakajima & Maiolino 2022).

The aim of this paper is to build on previous works by providing a comprehensive overview of the capabilities of *JWST* in observing and identifying Pop III galaxies. We wish to consider in detail the role of all four of *JWST*'s scientific instruments across all of their observing modes, from imaging to slitless and slit spectroscopy. Indeed, we intend this work to encompass all aspects of the observational Pop III search, from the initial identification of Pop III candidates using colour- and/or emission-line selections, to the removal of interlopers and stronger Pop III constraints derived from follow-up *JWST* spectroscopy. We present a series of photometric and spectroscopic diagnostics that have been designed to be as viable as possible, targeting photometric and spectral features that can be detected in relatively short integration times (compared to alternatives). Simultaneously, we aim for these diagnostics to still be effective and practical, offering valuable constraints once observational errors on e.g. colours or line fluxes, model uncertainties and potentially unknown source parameters (like the ionization parameter U, which is the ratio between the number density of ionizing photons and hydrogen atoms) are taken into account.

This paper is structured as follows. In Section 2, we discuss the models for Pop III (and non-Pop III) spectra that will be used in our analysis. In Section 3, we discuss the prospects of observing and identifying Pop III $z \sim 8$ galaxies with *JWST*. We discuss their expected apparent magnitudes and line fluxes, as well as the integration times needed to achieve a 5σ detection with imaging and slitless spectroscopy, as well as the visibility time-scales for Pop III galaxies. We introduce and discuss several colour selections for identifying Pop III candidates, as well as the prospects of identifying Pop III candidates from slitless spectroscopic emission-line surveys with *JWST*. We undertake a similar analysis of $z \sim 10$ Pop III galaxies in Appendix B. In Section 4, we discuss the additional Pop III constraints that can be derived from follow-up spectroscopy on Pop III candidates, as well as the integration times needed to achieve 5σ line detections with NIRSpec. In Section 5, we discuss our assumptions regarding the stellar mass of Pop III galaxies, their redshifts and the general likelihood of encountering Pop III galaxies with *JWST*. Finally, in Section 6, we summarize our main findings and conclude.

We assume a nominal stellar mass of $M_* = 10^6$ $M_\odot$ in our analysis, rather than the typical Pop III stellar mass of $M_* = 10^5$ $M_\odot$ expected from virial arguments. This nominal stellar mass was chosen as it likely reflects the least massive Pop III galaxies that will be detectable within feasible integration times with *JWST*. We adopt a Planck Collaboration (2020) cosmology.

2 POPULATION III MODELS

We make use of both the Zackrisson et al. (2011) and Nakajima & Maiolino (2022) models for Pop III (as well as non-Pop III) spectra in our analysis. This approach was adopted for two reasons. First, to investigate the robustness of our colour selections and spectroscopic diagnostics at identifying and confirming Pop III candidates. Secondly, to draw upon the synergy between these two different but complementary models. With the Zackrisson et al. (2011) models, we will determine the expected apparent magnitudes and line fluxes for $z = 8$ Pop III sources, as well as investigate the time-dependence of these quantities. With the Nakajima & Maiolino (2022) models, we explore the dependence of our emission line diagnostics on the ionization parameter U and push our analysis of non-Pop III galaxies down to even lower (but still non-pristine) metallicities. We refer the reader to the respective papers for the full details on these models. In this section, we briefly outline the features of these models that are most relevant for our analysis.

The Zackrisson et al. (2011) models provide rest UV-to-FIR spectra for both Pop III and non-Pop III populations. Most importantly, the spectra contain both stellar and nebular emission, with the pure stellar templates provided as inputs to the CLOUDY (Ferland et al. 1998) photoionization code (following the procedure in Zackrisson et al. 2001), which in turn computes the associated nebular continuum and line emission. Models with ISM covering fractions of $f_{\rm cov} = 0$, 0.5, 1 are provided. We use the $f_{\rm cov} = 1$ spectra in our analysis, though we refer to the $f_{\rm cov} = 0.5$ results when relevant.

For the Pop III galaxies, three different IMFs are available: Pop III.1, Pop III.2, and Pop III with a Kroupa IMF. Roughly speaking, the characteristic mass of stars $M_{*,\,\rm IMF}$ formed in the Pop III.1, Pop III.2, and Pop III Kroupa IMFs are $\sim$100, $\sim$10, and $\sim$1 $M_\odot$, respectively. In the case of Pop III.1, the Schaerer (2002) stellar SSP with a power-law IMF of slope $\alpha = 2.35$ across the mass range 50–500 $M_\odot$ is used. For Pop III.2 galaxies, the Raiter et al. (2010) model is adopted,

which has a log-normal IMF with characteristic mass $M_c = 10\,M_\odot$ and dispersion $\sigma = 1\,M_\odot$, with wings extending from 1 to 500 $M_\odot$. For the Pop III Kroupa galaxies (which we include for completeness, and as a reference against the non-Pop III models, which also have a Kroupa IMF), the Kroupa (2001) IMF is adopted. Zackrisson et al. (2011) model spectra for non-Pop III (i.e. Pop II and Pop I) galaxies are also analysed. These assume the Kroupa (2001) IMF and are provided at $Z = [0.02, 0.2, 0.4, 1]\,Z_\odot$.

The Nakajima & Maiolino (2022) models also provide rest UV-to-FIR spectra for both Pop III and non-Pop III populations, including both the stellar and nebular (generated using CLOUDY, Ferland et al. 1998, 2013) emission.

For their Pop III galaxies, three metal-free stellar populations from Schaerer (2003) and Raiter et al. (2010) are used. A Salpeter (1955) IMF is adopted, with three different mass ranges considered: 1–100, 1–500, and 50–500 $M_\odot$. Three gas-phase metallicities are also available: $Z_{gas} = 0, Z_\odot/1400, Z_\odot/140$. The non-zero metallicities are considered to explore the scenario of Pop III galaxies forming from pockets of pristine gas surviving in slightly enriched environments. We use the Nakajima & Maiolino (2022) Pop III spectra with electron density $n_e = 10^3\,cm^{-3}$, across the ionization parameter range $\log U = [-2.0, -1.5, -1.0, -0.5]$.

Metal-poor Pop II models are also provided, spanning the metallicities $Z = [Z_\odot/1400, Z_\odot/140, Z_\odot/14]$, and across the ionization parameter range $\log U = [-2.0, -1.5, -1.0, -0.5]$. BPASS SEDs with a Kroupa (2001) IMF with two possible upper mass limits are used, namely 100 and 300 $M_\odot$. Metal-enriched Pop I models are available at the following metallicities: $Z = [0.1, 0.2, 0.5, 1]\,Z_\odot$, and at the following ionization parameter values: $\log U = [-3.0, -2.5, -2.0, -1.5, -1.0, -0.5]$.

Model spectra for active galactic nuclei (AGN) and direct collapse black holes (DCBH) are also used, though these are not central to our analysis. We only comment that while both AGN and DCBH can have bright He II λ1640 emission (similar to Pop III galaxies), they have very distinct red colours and so would not be confused with Pop III systems, see Fig. A1 but also Inayoshi et al. (2022).

We use the Inoue et al. (2014) prescription for IGM attenuation in our analysis. This essentially removes all the flux blueward of the central wavelength of Lyα. Though we note that this prescription does not result in any attenuation/scattering redward of the Lyα peak. When discussing our colour selections in Section 3.2, the Inoue et al. (2014) IGM attenuation has been applied to the spectrum. However, when discussing spectroscopic diagnostics involving the Lyα line, as well as expected Lyα fluxes, we instead use the intrinsic (i.e. unattenuated) Lyα line.

Finally, we assume the Calzetti et al. (2000) dust attenuation law in this work. Although we do not explicitly apply this attenuation law to any of the model spectra, we do show the imprint that dust reddening would have on galaxy colours within the colour–colour plane.

3 THE OBSERVABILITY AND IDENTIFICATION OF POP III CANDIDATES

In this section, we discuss the prospects of observing and identifying Pop III candidates with *JWST*. Our analysis will focus on Pop III candidates at $z \sim 8$. We mirror this analysis for $z \sim 10$ candidates in Appendix B. In Section 3.1, we introduce the identifying, distinct features of a Pop III spectrum and the expected observability windows after a starburst. In Section 3.2, we discuss our colour–colour selections, outlining the principles behind these selections, the redshift windows of applicability and potential high-z and Galactic contaminants. Finally, in Section 3.3, we discuss the feasibility of identifying Pop III candidates in *JWST* slitless spectroscopic emission-line surveys.

3.1 Pop III spectrum and photometry

We show an example of the spectrum of a $\log(M_*/M_\odot) = 6$ Pop III galaxy at $z = 8$, together with its associated *JWST* NIRCam + MIRI photometry in Fig. 1. Here, we adopt the Pop III.1 model from Zackrisson et al. (2011), which corresponds to the most top-heavy Pop III IMF in their models. We show the expected spectrum immediately after (0.01 Myr) an instantaneous starburst. The *JWST* filters shown in Fig. 1 will be considered throughout our analysis in this paper. This set of NIRCam and MIRI filters has been chosen for two reasons. First, because these filters are likely to be the standard filter set used by *JWST*, having been widely adopted in Cycle 1 observations. Secondly, because we found that these filters proved to capture the most salient spectral features needed for Pop III identification.

In the following section, we briefly outline the key spectral features that distinguish Pop III galaxies from non-Pop III galaxies. This overview therefore forms the basis behind our subsequent colour and emission-line selections in Sections 3.2 and 3.3, as well as our recommendations for spectroscopic follow-up observations in Section 4.

3.1.1 Distinguishing Pop III spectral features

Owing to their metal-free nature, as well as their potentially more top-heavy IMF, Pop III stars (and galaxies) are expected to produce more ionizing photons per unit stellar mass than non-Pop III stars (e.g. Schaerer 2002, 2003; Raiter et al. 2010; Zackrisson et al. 2011). Hence, we expect the recombination lines of hydrogen and helium to have a greater luminosity per unit stellar mass for Pop III galaxies. Furthermore, the ionizing radiation produced will also be harder than for non-Pop III stars (e.g. Schaerer 2002, 2003), Hence, we also expect the recombination lines of doubly-ionized helium (He II) to have much greater luminosity per unit stellar mass for Pop III galaxies.

The great source of (hard) ionizing photons therefore heats more ISM to a greater temperature than for non-Pop III stars, resulting in a much brighter nebular continuum contribution to the total (stellar + nebular) Pop III spectrum (e.g. Zackrisson et al. 2001; Schaerer 2002; Zackrisson et al. 2011). Although the brightest stars in a Pop III population are bluer than their non-Pop III counterparts, the greater contribution from the relatively cooler and redder nebular continuum results in the total Pop III spectrum being redder than for non-Pop III stars, which manifests itself in, e.g. a less negative 1500 Å UV slope β (e.g. Raiter et al. 2010; Zackrisson et al. 2011; Dunlop 2013).

Given their higher ionizing photon production rate (and hence recombination rate), one might expect the Balmer and Paschen jumps to be larger (in terms of an AB magnitude difference blueward and redward of the jump) for Pop III galaxies. However, we found that these jumps are in fact weaker for Pop III galaxies. Given the higher ISM temperatures (e.g. Schaerer 2003), the recombining electrons in Pop III systems have a greater spread of energies, with a smaller fraction of particles therefore recombining with energy $E = 0$. Since it is precisely the recombination rate of the $E = 0$ particles that drive the jump strength, the Balmer and Paschen jumps are weaker for Pop III galaxies.

Finally, since Pop III galaxies are by definition metal-free, their spectra do not contain any metal emission- or absorption-lines.

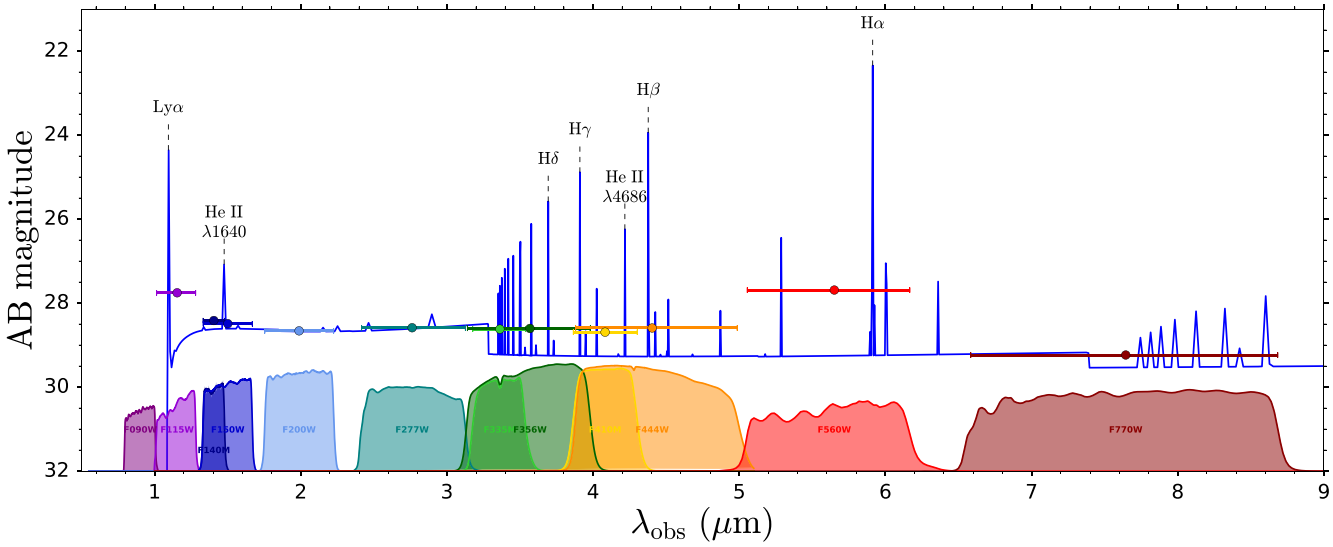

Figure 1. The spectrum of a $z = 8$ Pop III.1 galaxy (i.e. with the characteristic mass of the individual Pop III stars $M_{*,\,\rm IMF}$ being $\sim$100 $\rm M_\odot$) at the nominal stellar mass $\log(M_*/\rm M_\odot) = 6$, observed immediately after (0.01 Myr) an instantaneous starburst. The filter throughputs and bandpass-averaged flux densities within the *JWST* NIRCam + MIRI bands that are used throughout our $z \sim 8$ analysis are also shown.

Table 1. The expected apparent magnitudes in *JWST* NIRCam + MIRI bands (top row) and integration times needed (in hours) to achieve a 5σ detection (bottom row) for the three Zackrisson et al. (2011) Pop III models at $z = 8$ with $\log(M_*/\rm M_\odot) = 6$ observed immediately after (0.01 Myr) an instantaneous starburst. The time-scales (in Myr) over which the average magnitude for Pop III galaxies in the listed *JWST* bands drops by 0.25 and 1.0 mag are also provided, which should serve as an indication of the visibility window over which Pop III galaxies can be detected. Roughly speaking, the characteristic mass of stars $M_{*,\,\rm IMF}$ formed in the Pop III.1, Pop III.2, and Pop III Kroupa IMFs are $\sim$100, $\sim$10, and $\sim$1 $\rm M_\odot$, respectively. The integration times were estimated using the *JWST* ETC, assuming a point source, and adopting a 0.32 arcsec diameter circular extraction aperture for the NIRCam bands, and a 0.49 and 0.55 arcsec aperture for the MIRI *F560W* and *F770W* bands, respectively.

IMF	*F090W*	*F115W*	*F140M*	*F150W*	*F200W*	*F277W*	*F335M*	*F356W*	*F410M*	*F444W*	*F560W*	*F770W*	$\Delta m = 0.25$	$\Delta m = 1.0$
Pop III.1	38.15	27.75	28.41	28.49	28.66	28.58	28.62	28.60	28.69	28.59	27.69	29.23	2.2	2.8
($M_{*,\,\rm IMF} \sim 100$ $\rm M_\odot$)	N/A	0.40	1.73	0.94	0.81	0.75	1.61	0.66	2.45	1.34	10.57	691.86	–	–
Pop III.2	39.24	28.90	29.60	29.65	29.79	29.73	29.75	29.74	29.88	29.76	28.84	30.41	4.0	4.0
($M_{*,\,\rm IMF} \sim 10$ $\rm M_\odot$)	N/A	3.29	16.36	7.97	7.27	6.16	13.11	5.52	22.37	11.74	89.54	5970.61	–	–
Pop III Kroupa	41.13	30.86	31.55	31.58	31.72	31.68	31.71	31.71	31.87	31.75	30.84	32.40	4.0	5.6
($M_{*,\,\rm IMF} \sim 1$ $\rm M_\odot$)	N/A	121.78	593.99	284.17	254.43	227.81	475.96	203.97	858.17	450.37	3499.60	237694.36	–	–

Indeed, some of these metal emission-lines, such as the [O III] $\lambda\lambda$4959, 5007 and [S III] $\lambda\lambda$9069, 9531 doublets are relatively bright, and therefore have very high equivalent widths. As we shall see in Section 3.2, the absence of such bright lines in the Pop III spectrum can therefore lead to distinct colours that can be used to select Pop III candidates from photometry (see also Inoue 2011; Zackrisson et al. 2011).

3.1.2 The observability of Pop III galaxies

In Table 1, we show the expected AB magnitudes for Pop III galaxies at $z = 8$ with $\log(M_*/\rm M_\odot) = 6$ immediately after (0.01 Myr) an instantaneous starburst. We also show the expected integration times (in hours) needed to achieve a 5σ detection within the various NIRCam + MIRI bands. For this estimation, we use the *JWST* exposure time calculator (ETC; Pontoppidan et al. 2016), assuming a point source, and adopting a 0.32 arcsec diameter circular extraction aperture for the NIRCam bands, and larger apertures for the MIRI *F560W* (0.49 arcsec) and MIRI 770W (0.55 arcsec) bands, obtained by scaling the 0.32 arcsec diameter by the ratio between the FWHM of the respective MIRI filter and the NIRCam/*F444W* filter. Furthermore, in Fig. 2, we show how the apparent magnitudes of Pop III galaxies vary with time elapsed after an instantaneous starburst, showing both the bandpass-averaged flux densities in the *F115W* (purple) and *F444W* (orange) NIRCam filters (left-hand panel), as well as the bandpass-averaged flux densities in the *F560W* (red) and *F770W* (dark red) MIRI filters (right). These are compared against the expected, median 5σ depths achieved (horizontal dotted lines) with NIRCam (left) and MIRI (right) in integration times of 2.8 h = 10 ks, 25 h = *JWST* medium GO program, 75 h = *JWST* large GO program and 280 h = 1 Ms.

First, regarding detection with NIRCam, we see that Pop III galaxies with the more top-heavy III.1 and III.2 IMFs should be readily detectable at 5σ in medium-to-deep NIRCam surveys. On the other hand, Pop III galaxies with a Kroupa IMF will require extremely deep integrations ($\geq$100 h) to detect.

Secondly, detections with MIRI imaging will prove to be challenging. Detections in the F560W band will require long integrations (10–100 h), even for the Pop III.1 and Pop III.2 IMFs. 5σ detections in *F560W* for the Pop III Kroupa IMF, and in the *F770W* band for all three IMFs will likely be unachievable, given the exceptionally long integration times required ($\sim$1000 h).

However, the tabulated magnitudes and associated integration times assume an unlensed Pop III galaxy at the nominal stellar mass

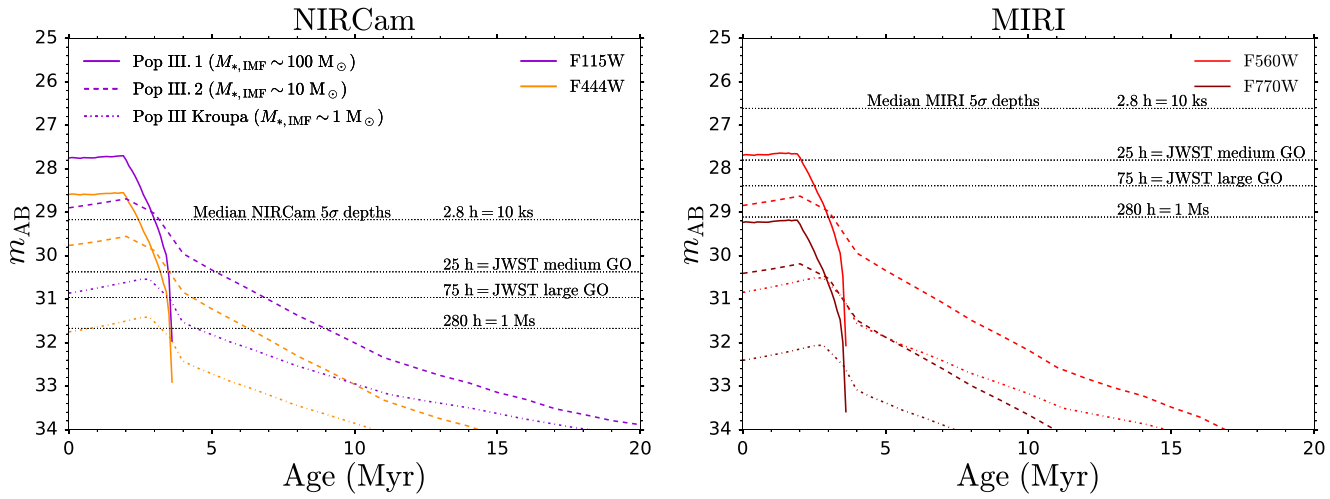

Figure 2. The apparent magnitudes of $z = 8$, $M_* = 10^6\,{\rm M}_\odot$ Pop III galaxies with three different IMFs (Pop III.1: solid; Pop III.2: dashed; Pop III Kroupa: dash–dotted) as a function of time elapsed after an instantaneous starburst. Left-hand panel: The bandpass-averaged flux densities in the NIRCam *F115W* (purple) and *F444W* (orange) filters. Right-hand panel: The bandpass-averaged flux densities in the MIRI *F560W* (red) and *F770W* (dark red) filters. Shown also are the expected 5σ depths achieved (horizontal dotted lines) with NIRCam (left) and MIRI (right) in integration times of 2.8 h = 10 ks, 25 h = *JWST* medium GO program, 75 h = *JWST* large GO program and 280 h = 1 Ms. Note that the NIRCam depths reflect the median depth of the *F115W*, *F150W*, *F200W*, *F277W*, *F335M*, *F356W*, *F410M*, and *F444W* filters. The MIRI depths reflect the median depth of the *F560W* and *F770W* filters. The elevated bandpass-averaged flux density in the *F115W* filter with respect to *F444W* (and the other NIRCam filters, which all have comparable flux densities, see Fig. 1 and Table 1) is due to the high EW Lyα line which resides in this filter at $z = 8$. Roughly speaking, the characteristic mass of stars $M_{*,\rm IMF}$ formed in the Pop III.1, Pop III.2, and Pop III Kroupa IMFs are ∼100, ∼10, and ∼1 ${\rm M}_\odot$, respectively.

of $\log(M_*/{\rm M}_\odot) = 6$. If there is a flux boost $b = \mu\mathcal{M}$ for the Pop III galaxy, either because of a magnification factor μ from gravitational lensing, or because the galaxy is a multiple $\mathcal{M} = M_*/10^6\,{\rm M}_\odot$ of the nominal stellar mass, then the required integration times will decrease. Assuming background-limited observations, the signal-to-noise S/N scales as ${\rm S/N} \propto f_{\rm cont}\sqrt{t}$, where $f_{\rm cont}$ is the continuum flux density in the appropriate *JWST* imaging band. Hence, with the flux boost b the new continuum level is $f'_{\rm cont} = bf_{\rm cont}$, and the required integration times become $t' = t/b^2$. Thus, with a flux boost factor $b = 10$, a 5σ detection of *F770W* for Pop III.1 and Pop III.2 starts to become a real possibility, as the integration times needed get pushed down to ∼7 and ∼60 h, respectively. Thus, deep MIRI imaging on gravitationally lensed fields (with $\mu = 10$) and/or fortuitous imaging of massive Pop III galaxies (with $\log(M_*/{\rm M}_\odot) = 7$) will be necessary to get valuable flux constraints from the *F770W* filter.

In Table 1, we also show the time-scales over which the average magnitude for Pop III galaxies in the listed *JWST* bands drops by 0.25 and 1.0 mag (following an instantaneous starburst), as an indication of the visibility window over which Pop III galaxies can be detected. Depending on the Pop III IMF, we see that the magnitudes remain roughly stable ($\Delta m = 0.25$) for 2.2–4.0 Myr, with their brightness having faded more strongly ($\Delta m = 1.0$) after 2.8–5.6 Myr. As we shall see in the next section on Pop III colour selection, Pop III galaxies maintain unique colours in the colour–colour plane over much longer time-scales than the aforementioned visibility windows. Hence, the limiting factor determining the time-scale over which Pop III galaxies can be identified is their visibility window (∼3 Myr), rather than the time window over which they exhibit unique colours (∼10–25 Myr).

3.2 Pop III galaxy colour selection

In this section, we introduce colour selections that can be applied to identify $z \sim 8$ Pop III candidates based off of their unique positions within colour–colour planes. In Section 3.2.1, we discuss what we believe to be the optimal Pop III colour selection, which is based off of both NIRCam and MIRI photometry. In Section 3.2.2, we discuss an alternative NIRCam + MIRI colour selection that can be more readily applied. In Sections 3.2.3 and 3.2.4, we discuss colour selections that only require NIRCam photometry. In Section 3.2.5, we briefly examine how effective measurements of the continuum slope, as inferred from photometry, will be at identifying Pop III candidates. Finally, in Section 3.2.6, we discuss the prospects for identifying Pop III galaxies through the imprint their high EW He II λ1640 emission leaves on NIRCam medium-band photometry.

3.2.1 [O III]−Hα, Hα −[S III] colour selection

Colour selection

We show the *F444W*−*F560W*, *F560W*−*F770W* colour–colour plane in Fig. 3. We note that this colour selection was also advocated for in Zackrisson et al. (2011). $z = 8$ Pop III galaxies are shown in blue, with the Pop III.1, Pop III.2, and Pop III Kroupa IMFs given by the dark blue solid, blue dashed and light blue dash–dotted curves, respectively. The $z = 8$ non-Pop III galaxies are shown in non-blue colours, with the $Z = [0.02, 0.2, 0.4, 1]\,Z_\odot$ metallicities, given by the green, yellow, orange and red points, respectively. The plus symbols represent the galaxy colours immediately after an instantaneous starburst, while the circles show the colours after subsequent 5 Myr intervals. We see that the Pop III galaxies occupy a unique region within the colour–colour plane immediately after the instantaneous starburst. Indeed, these unique colours are maintained for 10–25 Myr (thus much longer than the ∼3 Myr visibility windows following an instantaneous starburst discussed in Section 3.1.2). Furthermore, the non-Pop III galaxies do not overlap within this region, even long after the initial starburst. The basis behind this colour selection is as follows.

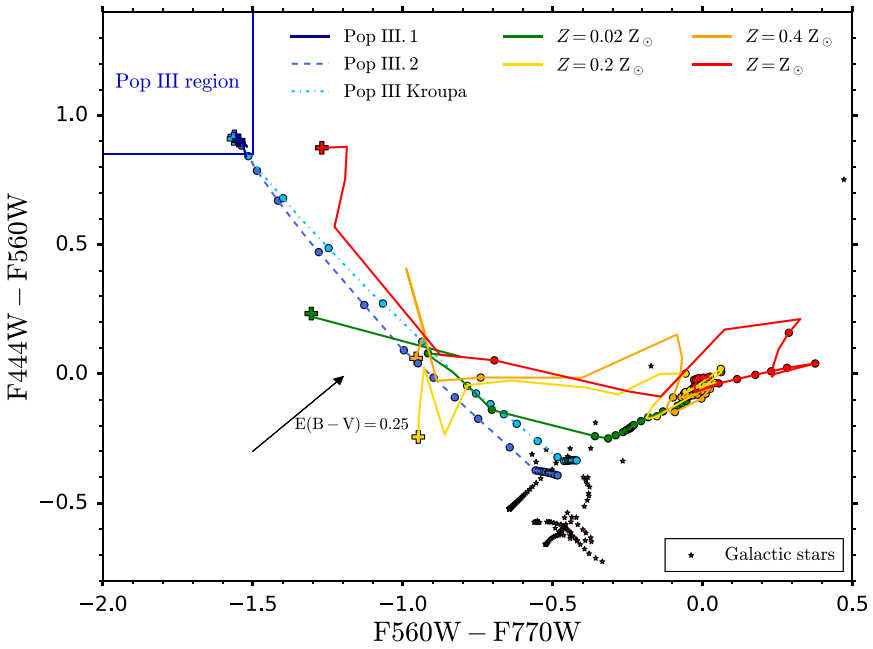

Figure 3. The *F444W*−*F560W*, *F560W*−*F770W* colour–colour plane for selecting $z \sim 8$ Pop III galaxies. The basis behind this selection is the marginally higher Hα EW for Pop III galaxies in the *F560W* filter, together with the lack of [O III] $\lambda\lambda$4959, 5007 and [S III] $\lambda\lambda$9069, 9531 emission in the *F444W* and *F770W* filters, respectively. We show the colours for $z = 8$ Pop III galaxies (different shades of blue) for three different IMFs: Pop III.1 (dark blue, solid), Pop III.2 (blue, dashed), and Pop III Kroupa (light blue, dash–dotted). Also shown are the colours for the $z = 8$ non-Pop III galaxies with $Z = 0.02\,Z_\odot$ (green), $Z = 0.2\,Z_\odot$ (yellow), $Z = 0.4\,Z_\odot$, (orange), $Z = Z_\odot$ (red). Plus symbols represent the galaxy colours immediately after an instantaneous starburst, while the circles show the colours after subsequent 5 Myr intervals up to 100 Myr. Note that the tracks for Pop III.1 galaxies (which overlap with Pop III.2 and Pop III Kroupa) are very short (and thus difficult to see in this figure and other colour–colour diagrams), as these dim rapidly after a starburst (see Fig. 2) and thus have no tabulated values beyond 3.6 Myr. The expected colours of Galactic stars (for both theoretical SEDs for very low-mass stars and brown dwarfs from Chabrier et al. 2000, as well as simple blackbody spectra) are indicated by the brown stars. The shift in colours due to dust reddening, assuming the Calzetti et al. (2000) attenuation law, is also given, with the length of the dust vector representing the colour shift associated with $E(B - V) = 0.25$. Pop III galaxies clearly occupy a unique region within this colour–colour plane, the boundaries of which are given by the solid blue lines (see text for more details on the Pop III region), and thus potential Pop III candidates can be identified through a colour selection. This colour–colour selection is applicable over the redshift range $7.55 < z < 8.10$. If contamination from $Z = Z_\odot$ galaxies is not deemed a concern, this selection can be applied over the wider redshift range $7.00 < z < 8.35$.

At $z = 8$, the Hα line falls in the MIRI F560W filter. As briefly outlined in Section 3.1.1, Pop III galaxies have higher Balmer recombination line luminosities per unit stellar mass. However, what is also the case is that the total (stellar + nebular) continuum is also higher per unit stellar mass. The net result, which will be discussed more in Section 4, is that the Hα equivalent width is only marginally higher ($\sim$0.1 dex) for Pop III galaxies. This therefore results in only a marginally higher ($\sim$0.15 mag) 'magnitude excess' in the *F560W* filter (akin to the more familiar IRAC excess), compared to for non-Pop III galaxies.

Additionally, at $z = 8$, the [S III] $\lambda\lambda$9069, 9531 doublets are redshifted into the MIRI *F770W* band. Although these lines are not very bright in terms of absolute brightness, they are bright relative to the rest-frame NIR continuum, having equivalent widths comparable to the more well-known [O III] $\lambda\lambda$4959, 5007 doublets in the rest-frame optical. Therefore, the [S III] doublets have a comparable effect on broad-band photometry to the [O III] doublets, generating a substantial magnitude excess in the *F770W* filter. $z = 8$ Pop III galaxies, with their marginally higher Hα EWs in *F560W* and lack of [S III] in *F770W*, thus have bluer *F560W*−*F770W* colours compared to non-Pop III galaxies.

Finally, at $z = 8$, the [O III] $\lambda\lambda$4959, 5007 doublet is redshifted into the NIRCam *F444W* band. This doublet drives a substantial magnitude excess in the *F444W* filter for non-Pop III galaxies. As a result, Pop III galaxies, with their lack of [O III] in *F444W*, and their marginally higher Hα EWs in *F560W* thus have redder *F444W*−*F560W* colours compared to non-Pop III galaxies.

Contamination

It is therefore the presence (or absence) of bright emission lines that is driving our colour selection in Fig. 3. The reason why both $Z = 0.02\,Z_\odot$ and $Z = Z_\odot$ galaxies have the most similar colours to Pop III is because their [O III] and [S III] emission lines have low EW. In the former case, this is because of the lack of metals, while in the latter it is due to the lack of ionization and/or heating of the ISM. Thus, whilst Pop III galaxies occupy a unique region within this colour–colour plane, they can start to become confused with $Z = 0.02\,Z_\odot$ and $Z = Z_\odot$ galaxies once observational errors on the measured colours are taken into account. Indeed, with only a 5σ detection in each filter comprising the colour pair, the colour uncertainty is $\sigma_C = 0.28$, and there can be some contamination of the Pop III region within the colour–colour plane. This contamination is largely eliminated with 10σ detections within each filter, but given the challenge of detecting Pop III galaxies with MIRI (see Section 3.1.2), this seems impractical to achieve.

Our colour selections in this work, with the exception of *F444W*−*F560W*, have been chosen such that Pop III galaxies exhibit

bluer colours than non-Pop III galaxies. This approach has been adopted for two reasons.

First, it ensures that non-Pop III galaxies, which can be reddened by dust, become even further separated from Pop III galaxies in the colour–colour plane. The shift in colour–colour caused by such reddening is shown by the reddening vector in each of our colour–colour diagrams.

Secondly, it ensures that the typical *red* contaminants that one encounters in high-z searches, such as Galactic brown dwarfs, Balmer break galaxies and dusty galaxies are not a concern. Instead, one must instead worry about potentially *blue* contaminants. At the long wavelengths typically probed by our colour selections, we capture the light redward of the blackbody peak in all but the coolest Galactic stars. Hence, these stars appear blue in e.g. the *F444W*−*F560W* and *F560W*−*F770W* colours. As can be seen from Fig. 3, there is no risk of confusing Pop III galaxies with Galactic stars, which are shown by the small brown star symbols and correspond to theoretical SEDs for very low-mass stars and brown dwarfs from Chabrier et al. (2000), as well as simple blackbody spectra spanning the temperature range $500 < T\,(\mathrm{K}) < 50\,000$.

The other potential contaminants would be blue, lower-z galaxies. In order to replicate the very blue *F560W*−*F770W* colours seen, these systems would have to have high EW emission lines that lie beyond Hα in the rest-frame. We found that the Paschen recombination lines (in the Zackrisson et al. 2011 models) simply do not have sufficient EW to achieve this, hence low-z contaminants are not a concern for this colour–colour selection. Indeed, assuming an otherwise flat f_ν SED, the magnitude excess Δm driven by emission lines in e.g. the *F560W* filter (yielding a blue *F560W*−*F770W* colour) is related to the total rest-frame equivalent width $\mathrm{EW_{tot,\,rest}}$ of all the emission lines that reside in the *F560W* filter, via $\Delta m = -2.5\log_{10}(1 + \mathrm{EW_{tot,\,rest}}(1 + z)/\Delta\lambda)$, where $\Delta\lambda$ is the bandpass width of the filter. Hence, a given observed blue *F560W*−*F770W* colour demands an increasingly higher rest-frame EW for contaminants at lower redshifts, which makes such low-z contaminants (such as $z \sim 2$ Paα emitters, which would require 3 × the rest-frame EW of $z \sim 8$ Hα emitters) unlikely in this case.

Regarding potential contaminants at *even higher* redshift, the only possibility would be $z \sim 10$ galaxies with bright [O III] emission in the *F560W* filter. However, as can be seen in Appendix B, although such galaxies can mimic the red *F444W*−*F560W* colours seen in $z \sim 8$ Pop III galaxies, they have relatively flat *F560W*−*F770W* colours (due to strong Hα emission in the *F770W* filter) compared to the blue colours seen in $z \sim 8$ Pop III galaxies. Hence, there is no risk of confusing $z \sim 8$ Pop III galaxies with $z \sim 10$ [O III] emitters in the *F444W*−*F560W*, *F560W*−*F770W* colour–colour plane.

Redshift range of applicability

We now comment on the redshift range over which these colour selections can be applied. In principle, this redshift range is set by the redshift interval over which the emission lines that drive the colour selection fall within the intended filters. In practice, however, the usable redshift range is narrower, as other (bright) emission lines get redshifted into and out of the adopted filters. This causes the locus of points occupied by Pop III and non-Pop III galaxies to drift in the colour–colour plane, causing overlap between Pop III and non-Pop III, and thus potential contamination.

We therefore find that the *F444W*−*F560W*, *F560W*−*F770W* colour selection can safely be applied over the redshift range $7.55 < z < 8.10$. Beyond this, redshift range $Z = Z_\odot$ galaxies begin to occupy the Pop III region within the colour–colour plane. However, if such high metallicity galaxies are not deemed a concern at $z \sim 8$, as one might not expect to find such enriched galaxies at these high redshifts (see e.g. Maiolino et al. 2008), then our colour selection can be applied over the broader redshift range $7.00 < z < 8.35$. A reliable assessment of the photometric redshift of Pop III candidates from their Lyα breaks will therefore likely be important to rule out potential high-z non-Pop III contaminants.

Pop III region

The solid blue lines in Fig. 3 denote our boundaries for what we define to be the 'Pop III region' of the *F444W*−*F560W*, *F560W*−*F770W* colour–colour plane. This is the range of colours that are uniquely exhibited by Pop III galaxies within the redshift range of applicability for this colour selection. When defining the extent of the Pop III region, we only consider the colours displayed by Pop III galaxies up to 5 Myr after the initial starburst, as beyond this time-scale Pop III galaxies (and their associated colours) are likely too faint to be observed with *JWST* (see Section 3.1.2). This is why the Pop III region does not encompass the full range of Pop III tracks in the *F444W*−*F560W*, *F560W*−*F770W* colour–colour plane. In defining the Pop III region, we have aimed to be as restrictive as possible, by keeping the Pop III region as small as possible. Our priority is to minimize the risk of contamination, which comes at the cost of completeness, as we will likely miss some real Pop III galaxies in the *JWST* data (as these get scattered out of the Pop III region by observational error or model uncertainties). We leave the boundaries of the Pop III region open-ended if we deem there to be little risk of contamination on the open side.

The boundaries of the Pop III region in the *F444W*−*F560W*, *F560W*−*F770W* colour–colour plane are given by:

$$\begin{aligned} F444W - F560W &> 0.85 \\ F560W - F770W &< -1.5 \end{aligned} \tag{1}$$

If contamination by $Z = Z_\odot$ galaxies is not deemed a concern, these boundaries can be extended to:

$$\begin{aligned} F444W - F560W &> 0.75 \\ F560W - F770W &< -1.25 \end{aligned} \tag{2}$$

We wish to stress that the identification of potential Pop III candidates through an application of the Pop III region criterion should be done with caution. Within the redshift range of applicability, the only galaxies (within the Zackrisson et al. 2011 models) that can exhibit colours within the Pop III region of the colour–colour plane are Pop III galaxies (by definition, and ignoring observational error). However, as discussed earlier, it is possible for *non*-Pop III galaxies *outside* of this redshift range (and Galactic stars) to have colours that lie *within* the Pop III region. Whenever applicable, we discuss these potential contaminants in the text and provide recommendations on how to distinguish them from actual Pop III galaxies. Additionally, the Pop III regions defined in this work were established by only considering the (limited) set of metallicities and galaxy properties probed by the Zackrisson et al. (2011) models. Hence, it is possible that the Pop III regions we have defined suffer from more contamination than what is explored here. Additionally, owing to model uncertainties, different Pop III (and non-Pop III) models likely predict different locations for the Pop III region in the colour–colour plane.

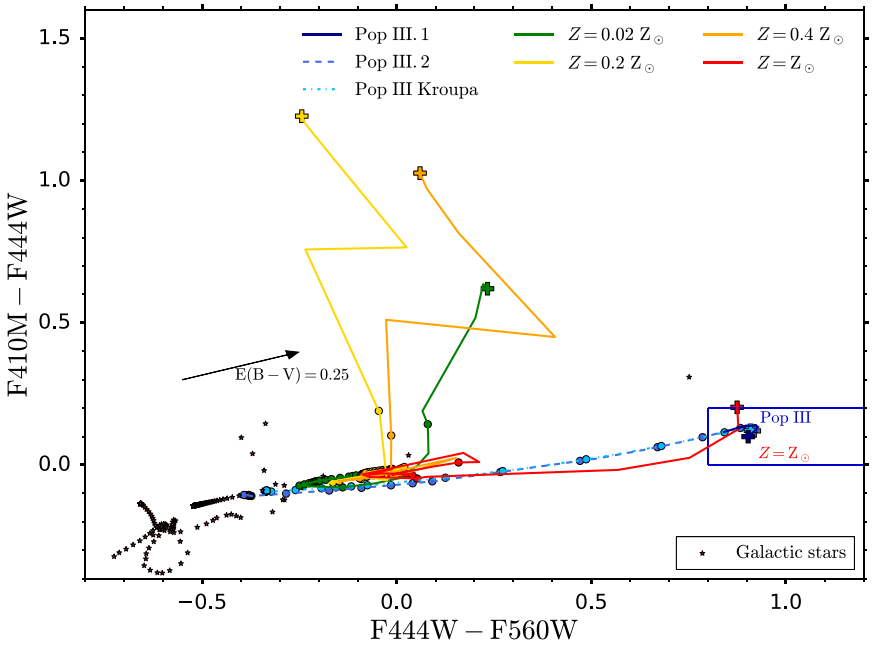

Figure 4. Similar to Fig. 3, but now showing the *F410M*−*F444W*, *F444W*−*F560W* colour–colour plane. The basis behind this selection is similar to Fig. 3, though the MIRI *F770W* filter (which was probing [S III]) has been substituted with the much more sensitive NIRCam *F410M* filter (which is now probing the continuum level around [O III] at $z \sim 8$, although *F356W* can also be adopted). Hence, this colour selection is more practical to apply, as the integration times needed to detect Pop III galaxies in all of the adopted filters (most notably *F560W*) are much shorter. Therefore, this colour selection does not require as substantial of a flux boost from gravitational lensing and/or elevated Pop III stellar masses to be applied. The drawback of this colour selection is the potential confusion between Pop III galaxies and $Z = Z_{\odot}$ galaxies, which have comparable colours. This redshift selection can be applied over the redshift interval $7.90 < z < 8.30$, with contamination by $Z = Z_{\odot}$ galaxies being a potential concern over this entire redshift range. The alternative colour selection, which uses *F356W* rather than *F410M* (i.e. *F356W*−*F444W*, *F444W*−*F560W*) can be applied over the wider redshift range $7.20 < z < 8.30$, but still suffers contamination by $Z = Z_{\odot}$ galaxies.

Caveats

Finally, we comment on the robustness of these colour selections. In Appendix A, we show the same colour–colour plane but applied to the Nakajima & Maiolino (2022) models. Qualitatively, we obtain similar results to what was obtained using the Zackrisson et al. (2011) models. There are minor quantitative differences regarding the positions of Pop III galaxies in the colour–colour plane, owing to differences in the spectral shapes and the EWs of the relevant emission lines between the Zackrisson et al. (2011) and Nakajima & Maiolino (2022) models. As the Nakajima & Maiolino (2022) models extend below $Z = 0.02\,Z_{\odot}$, we find that our adopted colour selections likely also pick up $Z \leq Z_{\odot}/140$ galaxies (even in the absence of any observational error). However, as we will discuss in Section 4, deep follow-up spectroscopy will enable us to definitively distinguish between Pop III and very metal-poor galaxies.

We note that our colour selections assume a covering fraction $f_{\rm cov} = 1$. Since these colour selections are primarily driven by the presence (or absence) of bright emission lines in the adopted filters, the resulting colours are sensitive to the strength of the emission lines and thus the covering fraction. For example, if we instead assume a covering fraction $f_{\rm cov} = 0.5$, then the emission line fluxes and equivalent widths will be smaller, resulting in a shift of the Pop III and non-Pop III regions in the colour–colour plane. Since the offset between Pop III and non-Pop III galaxies is due to their difference in emission line strength, this will also result in a reduced separation between Pop III and non-Pop III galaxies in the colour–colour plane. Therefore, while our colour selections are in principle effective at identifying Pop III candidates with $f_{\rm cov} = 1$, they may miss Pop III galaxies with lower covering fractions, as these could potentially overlap with the non-Pop III regions in our $f_{\rm cov} = 1$ colour–colour planes.

3.2.2 *[O III], [O III]−Hα colour selection*

Due to the weaker sensitivity of the MIRI *F770W* filter, together with the lack of bright H/He emission lines in this filter at $z \sim 8$ (as Hα instead resides in the MIRI *F560W* filter at $z \sim 8$) and lower continuum level, it will likely be very challenging to actually detect Pop III galaxies in the MIRI *F770W* filter (see Table 1 and Fig. 2). Thus, we introduce an alternative colour selection in Fig. 4, that is still rather robust (barring any contamination from $Z = Z_{\odot}$ galaxies), but much more practical to apply in practice. We substitute the MIRI *F770W* filter for the much more sensitive NIRCam *F410M* filter (though the *F356W* filter can also be used). Thus, this colour selection does not require as considerable of a flux boost from gravitational lensing or elevated Pop III masses to be applied. Here, we use the *F410M*−*F444W*, *F444W*−*F560W* filter pairs for our colour–colour selection. The basis behind this Pop III colour selection is as follows.

As outlined earlier, [O III] λ5007 resides in the *F444W* filter at $z = 8$. The *F410M* filter is chosen because it contains no bright metal emission lines and just measures the continuum level. Hence, at this redshift, the *F410M*−*F444W* colour is sensitive to the equivalent width of [O III]. This colour is therefore red for non-Pop III galaxies and relatively flat for Pop III galaxies as there is no oxygen. As before, Hα resides in the *F560W* filter, with the *F444W*−*F560W* colour being relatively red for $z \sim 8$ Pop III galaxies.

We note that the *F356W* filter could be adopted instead of *F410M*. The benefit of selecting the wide-band filter is that it is more sensitive and can be used over a wider redshift interval. Indeed, [O III] λ5007 resides in the *F410M* filter at $6.8 < z < 7.6$, which drives *blue* (rather than red) *F410M−F444W* colours for non-Pop III galaxies in that redshift range. Accounting for the effects of dust reddening and observational error on the measured colours, as well as uncertainties on the measured photometric redshifts, such galaxies could be confused with $z \sim 8$ Pop III galaxies, which is why the *F410M* filter can only be used over a narrower redshift interval. The drawback of using the alternative *F356W* filter is that it also contains the [O II] λλ3726, 3729 lines at $z \sim 8$, which therefore diminishes the impact of [O III] in driving redder colours in non-Pop III galaxies, thus reducing the separation between Pop III and non-Pop III galaxies in the colour–colour plane.

The *F410M−F444W*, *F444W−F560W* colour selection can be applied over the redshift interval $7.90 < z < 8.30$. Owing to their similar *F410M−F444W* and *F444W−F560W* colours to Pop III galaxies, contamination from $Z = Z_{\odot}$ galaxies may be a concern over this entire redshift range. The alternative *F356W−F444W*, *F444W−F560W* colour selection can be applied over the wider redshift range $7.20 < z < 8.30$ (but still suffers contamination by $Z = Z_{\odot}$ galaxies).

Furthermore, [O III] emitters at $9.15 < z < 11.40$ are also likely contaminants, due to their strong [O III] emission in the *F560W* filter, together with their relatively flat *F410M−F444W* colours, thus mimicking the colours of $z \sim 8$ Pop III galaxies. Given that these [O III] emitters are at higher redshift, they should in principle (barring any strong Lyα emission, see the next section) exhibit a stronger Lyα break in the *F115W* filter, being partial or even full *F115W* dropouts (*F115W−F150W* ≥1.5), as opposed to the $z \sim 8$ Pop III galaxies which should only exhibit minor IGM attenuation (*F115W−F150W* ≤0.5) in the F115W filter.

The boundaries of the Pop III, $Z = Z_{\odot}$ region in the *F410M−F444W*, *F444W−F560W* colour–colour plane are given by:

$$\begin{aligned} &0.0 < F410M - F444W < 0.2 \\ &F444W - F560W > 0.8 \end{aligned} \tag{3}$$

The boundaries of the Pop III, $Z = Z_{\odot}$ region in the alternate *F356W−F444W*, *F444W−F560W* colour–colour plane are instead:

$$\begin{aligned} &-0.15 < F356W - F444W < 0.1 \\ &F444W - F560W > 0.8 \end{aligned} \tag{4}$$

3.2.3 [O III], Lyα colour selection

Colour selection

Given NIRCam's greater sensitivity and imaging footprint (9.7 arcmin^2 versus 2.35 arcmin^2) compared to MIRI, we now discuss alternative colour selections that only require NIRCam photometry. We show our *F410M−F444W*, *F115W−F150W* colour selection in Fig. 5. The basis behind this colour selection is as follows.

At $z = 8$, the Lyα line falls within the *F115W* filter. Unlike the Balmer recombination lines, and which we shall discuss more extensively in Section 4, the equivalent width of Lyα is substantially higher for Pop III galaxies compared to non-Pop III. Hence, the magnitude excess in the *F115W* filter caused by Lyα is much greater for Pop III galaxies. The *F150W* filter is chosen to measure the neighbouring continuum level, with the *F115W−F150W* colour thus being sensitive to the EW of Lyα. Hence, Pop III galaxies will have bluer *F115W−F150W* colours than non-Pop III galaxies as they have a larger Lyα EW.

This colour selection can be applied across the redshift range $8 < z < 9$. The alternative *F356W−F444W*, *F115W−F150W* colour selection can be applied over the wider redshift range $7.50 < z < 9.00$.

The boundaries of the Pop III region in the *F410M−F444W*, *F115W−F150W* colour–colour plane are given by:

$$\begin{aligned} &-0.05 < F410M - F444W < 0.20 \\ &F115W - F150W < -0.6 \end{aligned} \tag{5}$$

The boundaries of the Pop III region in the alternative *F356W−F444W*, *F115W−F150W* colour–colour plane are instead:

$$\begin{aligned} &-0.15 < F356W - F444W < 0.10 \\ &F115W - F150W < -0.6 \end{aligned} \tag{6}$$

Contamination

Galactic stars are not likely potential contaminants. Any stars that have comparable *F410M−F444W*, *F115W−F444W* colours to Pop III galaxies (such as those in the lower left region of Fig. 5) should be able to be identified as such from an inspection of their full SED. Additionally, starburst galaxies at $z \sim 0.75$ with bright Hα emission in the *F115W* filter can mimic the colours of $z \sim 8$ Pop III galaxies. However, continuum detections in *F090W* and bluer, non-*JWST* filters should enable one to distinguish between $z \sim 8$ galaxies (which are non-detected in those bands) and these low-redshift interlopers.

Lyα attenuation

It should be noted that the colours shown in the top panel of Fig. 5 were obtained by applying the Inoue et al. (2014) prescription for IGM attenuation to the Zackrisson et al. (2011) spectra. This IGM attenuation essentially removes all flux blueward of the central wavelength of Lyα. However, it does not account for any scattering/attenuation of the flux redward of the Lyα peak, which can substantially diminish the total line flux that will actually be seen in observations. Indeed, Castellano et al. (2022) showed that galaxies in the epoch of reionization first need to carve out an ionizing bubble of radius 1 Mpc before Lyα is able to effectively escape. Given the Pop III visibility window (following an instantaneous starburst) of ∼3 Myr, this is insufficient time for ionizing photons to traverse such a distance, let alone completely ionize the gas enclosed in this volume. Hence, the true Lyα flux observed will likely be substantially less than what was adopted to generate the *F115W−F150W* colours in Fig. 5. Hence, in practice this colour selection may not be effective at identifying Pop III galaxies, as we will no longer be sensitive to the *intrinsic* Lyα EW.

We do note, however, that in most models, Pop III galaxies form because minihalos ($M_{\rm h} \sim 10^5$–10^6 M$_{\odot}$, which are otherwise capable of H_2 cooling) get strongly irradiated by the Lyman–Werner radiation from nearby, metal-enriched galaxies (e.g. Stiavelli & Trenti 2010) or quasars (e.g. Johnson & Aykutalp 2019), which prevents any star formation within these systems until they reach the H I cooling mass ($M_{\rm h} \sim 10^7$–10^8 M$_{\odot}$). Thus, these nearby galaxies/quasars may have contributed to the growth of an ionizing bubble that would allow Lyα to escape from Pop III galaxies. In this case, the Lyα flux should not be as heavily attenuated, suggesting that our aforementioned colour

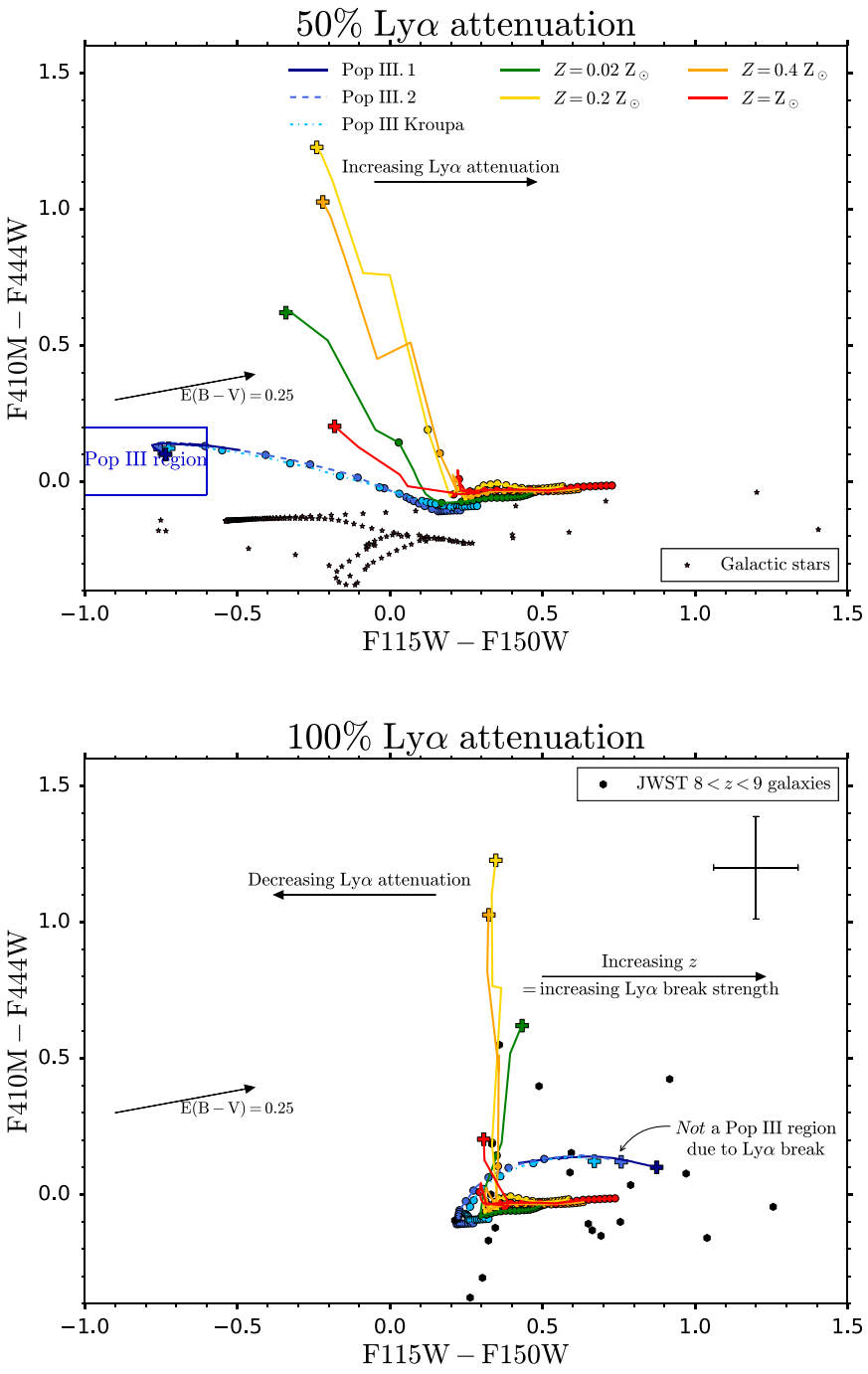

Figure 5. Top panel: Similar to Fig. 3, but now showing the *F410M−F444W*, *F115W−F150W* colour–colour plane. The basis behind this selection is the substantially higher Lyα EW for Pop III galaxies in the *F115W* filter, together with the lack of [O III] λ5007 emission in the *F444W* filter. This colour selection is applicable over the redshift range $8.0 < z < 9.0$. Note that the Inoue et al. (2014) IGM attenuation has been applied, which effectively removes all flux blueward of the Lyα central wavelength. However, no attenuation/scattering redward of the Lyα centre has been applied (i.e. the Lyα attenuation is 50 per cent). Hence, in practice the Lyα line may be much more heavily attenuated than in our models (except when Pop III galaxies form in the vicinity of galaxies/quasars that have already carved out ionized bubbles that enable Lyα to escape), which will erode this Pop III signature and thus may render this colour selection ineffective at identifying Pop III galaxies from observational data. Bottom panel: The *F410M−F444W*, *F115W−F150W* colours when 100 per cent of the Lyα emission is attenuated. The *F115W−F150W* colours become more red due to the lack of Lyα emission in the *F115W* filter. We stress that the relatively red *F115W−F150W* colours for $z = 8$ Pop III galaxies with 100 per cent Lyα attenuation should *not* be used as a Pop III indicator, as *F115W−F150W* is also sensitive to the strength of the Lyα break and thus increases with increasing redshift, causing Pop III and non-Pop III galaxies to overlap in *F115W−F150W* colour. We also show the colour of $8 < z < 9$ galaxy candidates (black hexagons) observed with *JWST* in the CEERS field, and the median error bar on their colours. The colours of these candidates are consistent with strong attenuation of Lyα, and thus the *F410M−F444W*, *F115W−F150W* colour selection cannot be used to distinguish between Pop III and non-Pop III galaxies.

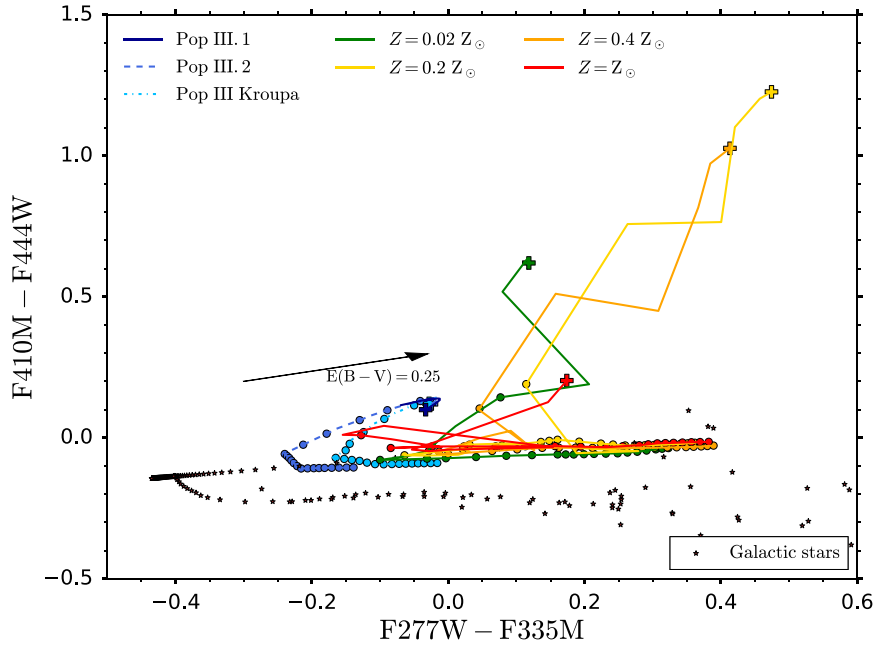

Figure 6. Similar to Fig. 3, but now showing the *F410M−F444W*, *F277W−F335M* colour–colour plane. The basis behind this selection is the lack of [O III] λ5007 and [O II] emission for Pop III galaxies in the *F444W* and *F335M* filters, respectively. This colour selection is applicable over the redshift range $7.95 < z < 8.35$, and is readily contaminated by other sources with flat colours. Owing to the limitations with this colour selection, we do not define a Pop III region to identify potential Pop III candidates in this colour–colour plane.

selection should in principle still be effective at identifying such Pop III galaxies.

We show the effect of increasing the Lyα attenuation to 100 per cent (up from 50 per cent) in the bottom panel of Fig. 5. The *F115W−F150W* colours clearly become more red due to the lack of Lyα emission in the *F115W* filter. We stress that the relatively red *F115W−F150W* colours for $z = 8$ Pop III galaxies with 100 per cent Lyα attenuation (compared to non-Pop III) should *not* be used as a Pop III indicator. The reason for this is that at $7.5 < z < 9.5$, the *F115W−F150W* colour is sensitive to the strength of the Lyα break, and thus becomes increasingly more red with increasing redshift (up to $z = 9.5$) as the Lyα break occupies progressively more of the *F115W* filter. Hence, the red colours of $z = 8$ Pop III galaxies with 100 per cent Lyα attenuation can overlap with those of non-Pop III galaxies at slightly higher redshift (than the $z = 8$ galaxies shown in Fig. 5). Hence, the *F115W−F150W* colour cannot be used to distinguish between Pop III and non-Pop III galaxies in the case of substantial Lyα attenuation.

Comparison against early JWST galaxies

We examine whether any potential Pop III candidates are present in the early *JWST* data, by showing the colours for $8 < z < 9$ galaxy candidates observed with *JWST* in Fig. 5. These galaxy candidates were imaged as part of the CEERS ERS program (Bagley et al. 2023a), using both the June 2022 and December 2022 data. Briefly, the NIRCam data was reduced following the procedure in Adams et al. (2023a), Adams et al. (2023b), and Ferreira et al. (2022), sources were identified using SExtractor (Bertin & Arnouts 1996) and photometric redshifts were derived using LePhare (Arnouts et al. 1999; Ilbert et al. 2006) and EAZY (Brammer, van Dokkum & Coppi 2008). Colours were measured from our calibrated photometry using the post-launch zero-points, e.g. Adams et al. (2023a).

The $8 < z < 9$ galaxy candidates shown in Fig. 5 were selected by requiring a $\geq 5\sigma$ detection in the filters comprising the colour selection, non-detections (i.e. $<2\sigma$) in the *HST* F606W and F814W bands (using *HST* data from the public CANDELS-EGS catalogs of Stefanon et al. 2017), as well as a best-fit photometric redshift $8 < z_{\rm phot} < 9$.

We see that the *F115W−F150W* colours of these $8 < z < 9$ galaxy candidates are consistent with strong attenuation of Lyα, and thus the *F410M−F444W*, *F115W−F150W* colour selection cannot be used to easily distinguish between Pop III and non-Pop III galaxies. Hence, it is not possible to establish whether any Pop III candidates are present in the data. However, these galaxies do generally fall in the region of where we find galaxies with normal stellar populations. This example shows how difficult it can be to use purely photometry to find Pop III galaxies, and likely several avenues will need to be investigated to verify any given system as Pop III.

3.2.4 *[O III], [O II] colour selection*

In order to highlight the prospects (or lack thereof) of identifying Pop III candidates through colour selections that target weaker (i.e. lower EW) metal emission lines, we show our final colour–colour selection in Fig. 6. Here, the *F410M−F444W*, *F277W−F335M* colour pairs have been adopted. At $z = 8$, the [O II] λλ3726, 3729 doublet resides in the *F335M* filter, while the *F277W* filter contains no bright metal lines and just measures the continuum level. Hence, the *F277W−F335M* colour is sensitive to the [O II] EW and will be red for non-Pop III galaxies and relatively flat for Pop III galaxies. Here, the less-used *F335M* filter was adopted, rather than the standardly used *F356W*, because the medium-band *F335M* filter will be more sensitive to the (rather weak) [O II] doublet.

This colour selection has two main drawbacks. First, it is only applicable over the narrow redshift range $7.95 < z < 8.35$. Secondly,

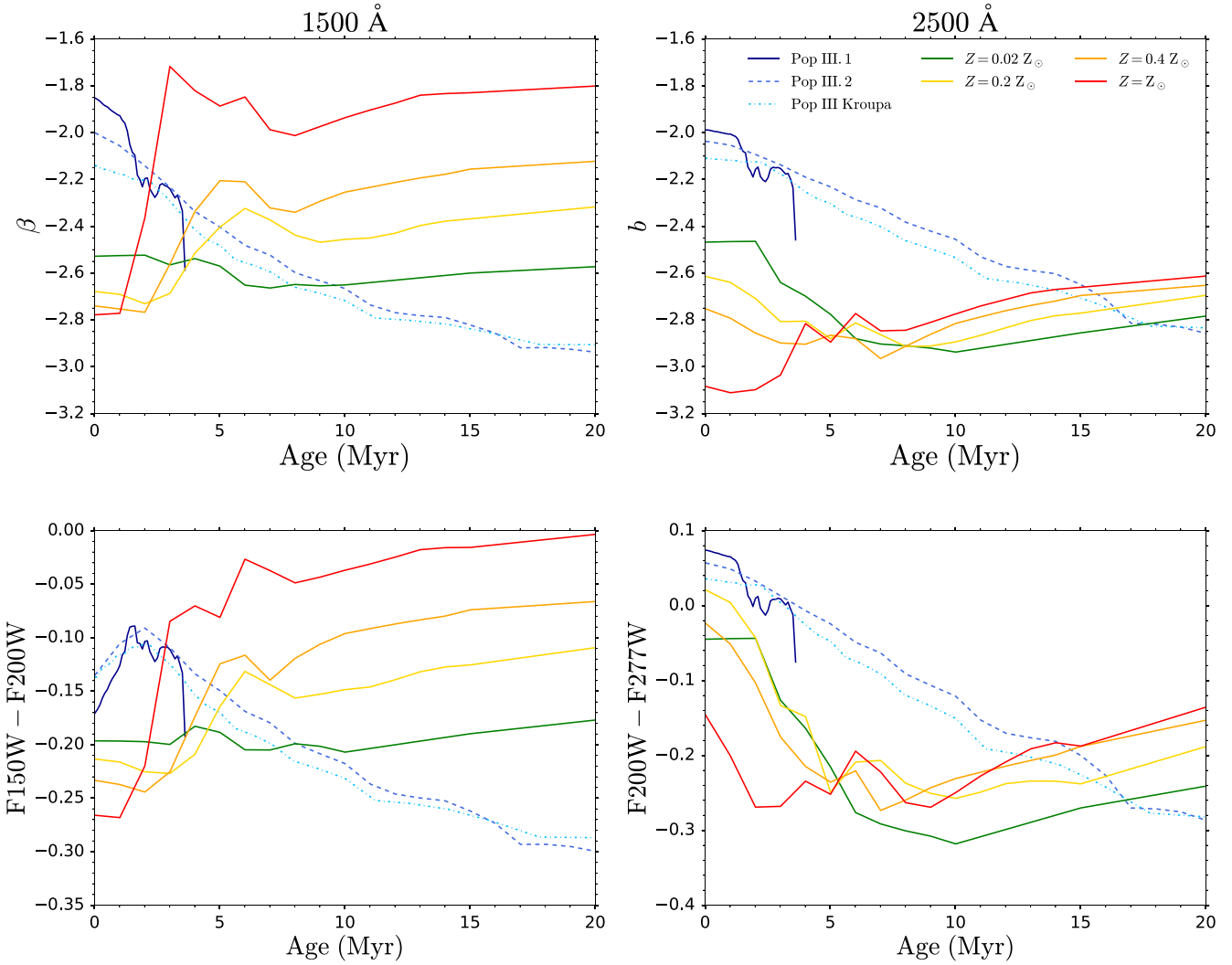

Figure 7. The UV 1500 Å continuum slope β (top left-hand panel) and 2500 Å continuum slope b (top right). Bottom panels: The imprint of the UV 1500 Å continuum slope and 2500 Å slope on NIRCam colours in the corresponding filters (*F150W−F200W* for 1500 Å, *F200W−F277W* for 2500 Å) for $z = 8$ galaxies. The ages refer to the time elapsed after the instantaneous starburst. The colour coding and line styles follow the format of Fig. 3. Note that Pop III galaxies actually have redder continuum slopes than non-Pop III galaxies. The imprint of these redder continuum slopes on NIRCam colours is likely too small (immediately after a starburst) to use these colours as a Pop III diagnostic in practice, as even a minor amount of dust reddening and colour measurement error ($\sigma_C = 0.28$ for 5σ flux density detections) will cause the Pop III and non-Pop III colours to overlap.

the flat Pop III colours in both filter pairs means that this region of the colour–colour plane can readily be contaminated by other sources. At late times after the initial starburst, both the [O II] and [O III] lines will have faded and non-Pop III $z \sim 8$ galaxies will have rather flat colours. Additionally, other sources at a diverse range of redshifts are likely to also have similar flat colours in these filter pairs.

Owing to the limitations with this colour selection, we therefore do not define a Pop III region to identify potential Pop III candidates in this colour–colour plane.

3.2.5 *Continuum slope selection*

In this selection, we briefly examine how effective measurements of the continuum slope, as inferred from photometry, will be at identifying Pop III candidates. We show the well-known UV power law index, i.e. the 1500 Å UV slope β in the top-left-hand panel of Fig. 7. Given *JWST*'s extensive coverage and sensitivity in the near- and mid-infrared, we will now be capable of probing the continuum slope at longer wavelengths than was possible before. Hence, in the top-right-hand panel we now introduce the new 2500 Å slope b, with this wavelength range being selected for two reasons. First, because it is relatively sensitive to Pop III stars. Secondly, because this region of the rest-frame spectrum is mostly devoid of high EW emission lines (with the possible exception of Mg II at ∼2800 Å), which would otherwise distort the inferred spectral slope.

As has already been pointed out in e.g. Raiter et al. (2010), Zackrisson et al. (2011), and Dunlop (2013), the UV slope β (and the 2500 Å slope b) are in fact *higher*, i.e. the spectrum is *more red*, for Pop III galaxies. Despite the fact that the most luminous Pop III stars will be hotter and therefore bluer than their non-Pop III counterparts, the very bright but relatively red nebular continuum emission, which is very notable in Pop III spectra, is ultimately what drives the redder UV and 2500 Å slopes in Pop III galaxies.

In the bottom panels, we show the likely inferences that can be made on the 1500 and 2500 Å slopes from measurements with

NIRCam photometry. At $z = 8$, the 1500 and 2500 Å rest-frame wavelengths get redshifted to 1.35 and 2.25 μm, respectively. Thus, we adopt the nearest accessible NIRCam filters available (avoiding *F115W* as it resides on Lyα), namely the *F150W*−*F200W* and *F200W*−*F277W* filter pairs. The expected colours in these NIRCam filters can roughly be estimated by assuming the continuum f_ν follows a power law: $C = m_\mathrm{b} - m_\mathrm{r} = -2.5\log(A\lambda_\mathrm{b}^n / A\lambda_\mathrm{r}^n) = -2.5n\log(\lambda_\mathrm{b}/\lambda_\mathrm{r})$. Here, n is the power law index, λ_b and λ_r are the effective wavelengths in the blue and red filters defining the colour C, with A being the power law normalization constant. In practice, if we wish to separate Pop III galaxies from non-Pop III, we are interested in the colour difference $\Delta C = -2.5\Delta n \log(\lambda_\mathrm{b}/\lambda_\mathrm{r})$.

As can be seen from Fig. 7, in practice these colour shifts are rather small (immediately after a starburst), being only ∼0.05–0.1 mag. This is in part due to the He II λ1640 line, which falls in the *F150W* filter, thus driving bluer-than-otherwise Pop III *F150W*−*F200W* colours. Furthermore, the Mg II ∼2800 Å doublet, which falls in the *F277W* filter, drives redder-than-otherwise non-Pop III *F200W*−*F277W* colours. Given the marginally *redder* Pop III colours, this small signal will likely be erased by even a minor amount of dust reddening. Additionally, assuming 5σ detections in the NIRCam filters, the colour uncertainty $\sigma_\mathrm{C} = 0.28$, which likely renders this Pop III colour diagnostic impractical.

3.2.6 *He II λ1640 medium-band selection*

As discussed in the literature (e.g. Schaerer 2002, 2003; Raiter et al. 2010), and in more detail in Section 4.3, high EW He II λ1640 emission likely serves as the definitive Pop III indicator. Thus, in this section, we highlight the prospects of identifying Pop III candidates at $z \sim 9$ through NIRCam medium-band imaging campaigns that target the He II λ1640 emission from Pop III galaxies. Although the EW of He II λ1640 is *relatively* high for Pop III galaxies, it is still small in an absolute sense, typically ranging from roughly 10–100 Å across different Pop III models and IMFs. Hence, the added emission line sensitivity from medium-band imaging (over a wide-band) will likely be crucial for identifying such emission lines through photometry, if possible. The expected magnitude excess driven by $z = 9$ He II λ1640 emission in the *F162M* filter (which we discuss below) is 0.30 mag for Pop III.1 galaxies (which have rest-frame He II λ1640 EW of 50 Å), and 0.48 mag for the highest EW He II λ1640 Pop III galaxies in the Nakajima & Maiolino (2022) models (with rest-frame EW of 80 Å).

At $z = 9$ (rather than our usual $z = 8$), He II λ1640 resides in the NIRCam *F162M* filter. As before, we seek neighbouring filters that probe the continuum level around He II λ1640, with the resulting colour thus being sensitive to the EW of the He II line, and thus in principle enabling one to distinguish between Pop III and non-Pop III galaxies. To find a way to identify these galaxies, we consider filters both redward and blueward of *F162M*, with Pop III galaxies having relatively blue and red colours in the corresponding *F162M* filter pairs, respectively. Owing to the intrinsically *bluer* UV slopes for non-Pop III galaxies (as discussed in the previous section), the filter used redward of *F162M* must be close in wavelength to *F162M*, otherwise Pop III and non-Pop III galaxies will exhibit similarly blue colours. We thus adopt the NIRCam *F182M* filter, rather than the *F200W* filter. Additionally, owing to the small wavelength gap between He II λ1640 and Lyα, it is in fact rather challenging to select a filter blueward of *F162M* that does not include Lyα (otherwise complicating the interpretation of the colour) and also does not cover He II λ1640 (otherwise weakening the Pop III colour signature). We thus adopt the NIRCam *F140M* filter (rather than the *F115W* or *F150W* filters).

We show the *F162M*−*F182M* and *F140M*−*F162M* colours of $z = 9$ galaxies in the left-hand and right-hand panels of Fig. 8, respectively. As mentioned above, although the He II λ1640 emission for Pop III galaxies drives a magnitude excess in the *F162M* filter, Pop III and non-Pop III galaxies have comparably blue *F162M*−*F182M* colours, due to the intrinsically bluer UV slopes of non-Pop III galaxies. In contrast, these bluer non-Pop III slopes help to increase the separation in *F140M*−*F162M* colour between Pop III and non-Pop III galaxies, with this colour therefore being a potentially viable Pop III indicator for galaxies at $z \sim 9$.

However, the *redder F140M*−*F162M* colours exhibited by Pop III galaxies can in principle be replicated by non-Pop III galaxies with a moderate amount of dust reddening. Indeed, although the *F140M* and *F162M* filters probe (at $z = 9$) the rather narrowly separated rest-frame wavelengths of 1400 and 1620 Å, respectively, most dust attenuation laws $k(\lambda)$ rise sharply with decreasing wavelength in this wavelength regime. Hence, the amount of dust reddening, i.e. colour excess $E(B-V)$, needed to shift ∼0.3 mag = $E(B-V)(k(1400\,\text{Å}) - k(1620\,\text{Å}))$, the non-Pop III galaxy *F140M*−*F162M* colours onto the Pop III is $E(B-V) = 0.35$, assuming the Calzetti et al. (2000) dust attenuation law.

Still, such dust-reddened non-Pop III galaxies should in principle be able to be distinguished from Pop III galaxies, from an inspection of their full SED, which should be relatively red. In the same vein, other potential contaminants such as C IV λλ1548, 1550 emitters (i.e. AGN or metal-poor galaxies, see e.g. Stark et al. 2015) or O III] λλ1661, 1666 emitters at comparable redshifts, can in principle also be removed (as these should have bright [O III] λ5007 emission). Indeed, by considering the entire SED (such as through SED fitting, which we will investigate in a future work), the inclusion of the *F140M* filter (or *F182M* filter) likely is not necessary to probe the He II λ1640 EW (at $z = 9$), as the presence (or absence) of a magnitude excess in the *F162M* filter should be able to be inferred from a comparison against the photometry in the other *JWST* bands.

Thus, owing to the enhanced sensitivity and footprint of NIRCam relative to MIRI, medium-band NIRCam imaging surveys that search for high EW He II λ1640 emitters may provide a viable alternative for identifying Pop III candidates to the deep *F560W* and *F770W* imaging campaigns with MIRI. However, it is likely that only Pop III galaxies with the most top-heavy IMFs (such as Pop III.1), imaged immediately after the starburst ($\Delta t < 1$ Myr) can be identified in this way.

In Table 2, we show the various NIRCam medium-bands that can be used to target He II λ1640 emitters at different redshifts, together with the expected apparent magnitudes, exposure times needed for 5σ detections, and the likely magnitude excess Δm in the medium-band, for the Zackrisson et al. (2011) Pop III models considered in this work. We note that the NIRCam *F140M*, *F162M*, *F182M*, and *F210M* bands can be used to target He II λ1640 (and thus Pop III, AGN or DCBH candidates, but also galaxies containing Wolf–Rayet stars and X-ray binaries, see e.g. Katz et al. 2023) at $z = 7.5$, 9, 10, and 12, respectively. The exposure times required to reach 5σ depth in the aforementioned filters are relatively short (compared to the MIRI requirements), at <4 and <40 h for the Pop III.1 and Pop III.2 IMFs, respectively. However, deeper imaging (going beyond 5σ depth, i.e. $\sigma_\mathrm{m} = 0.2$) will likely be required for the small photometric He II λ1640 signature we are searching for ($\Delta m \sim 0.15$–0.30 mag) to be convincing.

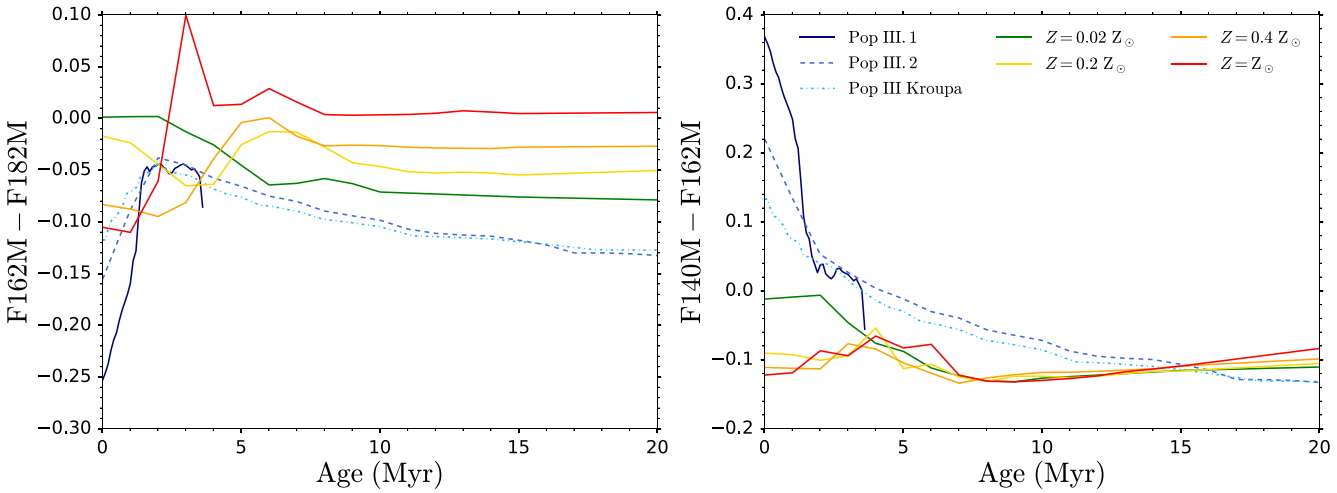

Figure 8. The *F162M*−*F182M* (left-hand panel) and *F140M*−*F162M* colours for $z = 9$ (rather than our usual $z = 8$) galaxies. At $z = 9$, the He II λ1640 line resides in the *F162M* filter. Thus, the *F162M*−*F182M* and *F140M*−*F162M* colours are in principle sensitive to the He II λ1640 EW at this redshift, which is characteristically high for Pop III galaxies. Despite the magnitude excess driven by He II λ1640 emission in the *F162M* filter for Pop III galaxies, the *F162M*−*F182M* colours for non-Pop III galaxies are comparably blue due to their intrinsically bluer UV continua. In contrast, these bluer non-Pop III UV slopes helps increase the separation in *F140M*−*F162M* colour between Pop III and non-Pop III galaxies, with this colour therefore being a potentially viable Pop III indicator for galaxies at $z \sim 9$. Dust-reddened non-Pop III galaxies, C IV λλ1548, 1550 emitters and O III] λλ1661, 1666 emitters are potential contaminants, though in principle these can be removed through an inspection of their full SED. Indeed, the inclusion of the *F140M* filter (or *F182M* filter) is likely not necessary to probe the He II λ1640 EW (at $z = 9$), as the presence of a *F162M* excess can be inferred from a consideration of the full SED, using the photometry in the other *JWST* bands. Thus, medium-band NIRCam imaging surveys (see Table 2) that search for high EW He II λ1640 emitters may provide a viable alternative for identifying Pop III candidates to deep and expensive *F560W* and *F770W* imaging campaigns with MIRI.

Table 2. The NIRCam medium-band filters that can be used to search for Pop III candidates by targeting their characteristically strong He II λ1640 emission. Also shown are the redshift ranges over which the respective filters can be applied, the expected apparent magnitudes in those filters (assuming a Pop III galaxy with $\log(M_*/\mathrm{M}_\odot) = 6$, imaged immediately after an instantaneous starburst), the exposure times (in hours) required to reach 5σ depth, as well as the approximate magnitude excess $\Delta m = 2.5\log_{10}(1 + \mathrm{EW}_{\mathrm{He\,II,\,rest}}(1+z)/\Delta\lambda)$ in the adopted filter. Here, $\Delta\lambda$ is the bandpass width of the filter, and the sources are assumed to be at $z = 7.5$, 9, 10, 12 for the *F140M*, *F162M*, *F182M*, and *F210M* filters, respectively. We assume He II λ1640 rest-frame equivalent widths $\mathrm{EW}_{\mathrm{He\,II,\,rest}}$ of 50, 26, 15 Å (see Section 4.3) for the Pop III.1, Pop III.2, and Pop III Kroupa IMFs, respectively.

Filter	Redshift range	IMF	Apparent magnitude (AB mag)	5σ exposure time (h)	Magnitude excess Δm
		Pop III.1	28.27	1.73	0.30
F140M	$7.10 < z < 8.00$	Pop III.2	29.49	16.36	0.15
		Pop III Kroupa	31.44	593.99	0.09
		Pop III.1	28.54	2.16	0.30
F162M	$8.40 < z < 9.45$	Pop III.2	29.75	20.03	0.15
		Pop III Kroupa	31.71	740.93	0.09
		Pop III.1	28.74	2.20	0.23
F182M	$9.50 < z < 11.00$	Pop III.2	29.94	20.03	0.12
		Pop III Kroupa	31.89	727.41	0.07
		Pop III.1	28.95	4.19	0.32
F210M	$11.15 < z < 12.40$	Pop III.2	30.17	39.61	0.16
		Pop III Kroupa	32.13	1464.80	0.09

3.3 Slitless emission-line-selection

In this subsection, we discuss the prospects for identifying Pop III candidates from blind emission-line surveys carried out through slitless spectroscopy with NIRISS ($0.8 \leq \lambda\,(\mu\mathrm{m}) \leq 2.0$) and NIRCam ($2.0 \leq \lambda\,(\mu\mathrm{m}) \leq 5.0$). We focus on the brightest lines that yield the greatest constraints on the potential Pop III nature of the galaxy. These lines are Hβ, Lyα, and He II λ1640. The expected line fluxes for $z = 8$ Pop III galaxies with $\log(M_*/\mathrm{M}_\odot) = 6$ detected immediately after an instantaneous starburst are shown in Table 3. We also include the expected integration times needed to achieve a 5σ line detection, estimated by extrapolating the exposure times and sensitivities reported for NIRISS and NIRCam in the NGDEEP survey (Bagley et al. 2023b) and the FRESCO survey (Oesch et al. 2023), respectively. We discuss the properties of these individual lines below and how well we can use these as a tracer of Pop III galaxies.

Table 3. The expected Hβ, *unattenuated* Lyα and He II λ1640 fluxes (in cgs units, i.e. erg s^{-1} cm^{-2}), as well as the integration times (in hours) needed to achieve a 5σ detection with NIRISS/NIRCam slitless spectroscopy, for the three Zackrisson Pop III models at $z = 8$ with $\log(M_*/M_\odot) = 6$ observed *immediately after* (0.01 Myr) an instantaneous starburst. The expected line fluxes and required integration times will be different (see the time evolution of the emission line luminosities in Section 4) if the Pop III galaxy is observed at a later time after the starburst. The integration times were estimated by extrapolating from the NIRISS and NIRCam sensitivities reported in Bagley et al. (2023b) and Oesch et al. (2023), respectively.

IMF	Hβ flux (cgs)	Hβ 5σ exposure time (h)	Lyα flux (cgs)	Lyα 5σ exposure time (h)	He II λ1640 flux (cgs)	He II λ1640 5σ exposure time (h)
Pop III.1	6.76×10^{-19}	17.12	3.31×10^{-17}	0.07	8.71×10^{-19}	55.25
Pop III.2	2.34×10^{-19}	142.92	1.10×10^{-17}	0.62	1.58×10^{-19}	1678.90
Pop III Kroupa	3.63×10^{-20}	5938.84	1.78×10^{-18}	23.72	1.58×10^{-20}	167889.76

3.3.1 Hβ detection

At $z = 8$, the Hβ line is redshifted to $\lambda = 4.37\,\mu$m, placing it within the *F444W* band for slitless spectroscopic observations with NIRCam. As can be seen from Table 3, the integration times needed for a 5σ detection are demanding (17.12, 142.92 h), even for the Pop III.1 and Pop III.2 IMFs. Of course, the integration times can be reduced substantially with moderate lensing μ and/or a mass boost $\mathcal{M}$ above the assumed nominal stellar mass.

As will be discussed more extensively in Section 4, the merits to detecting Hβ for Pop III identification are twofold. First, a measurement of the Hβ equivalent width can place constraints on the potential Pop III nature of the source, though in practice this will require a line detection at much more than just 5σ significance. Secondly, a non-detection of the neighbouring bright [O III] λ5007 line (which will also lie within the *F444W* band), can be used to place constraints on the upper limit of the metallicity of the galaxy (see also Nakajima & Maiolino 2022).

3.3.2 Lyα detection

At $z = 8$, the Lyα line is redshifted to $\lambda = 1.09\,\mu$m, placing it within the *F115W* band for slitless spectroscopic observations with NIRISS. The Lyα line fluxes in Table 3 correspond to the intrinsic line fluxes, i.e. assuming no IGM attenuation. In this case, the integration times needed are exceptionally short, owing to the great intrinsic brightness of this line for Pop III galaxies. In reality, Lyα will be heavily attenuated and scattered by the IGM. Thus, this line will actually be much fainter in observations, and may therefore be an unreliable Pop III indicator.

3.3.3 He II λ1640 detection

At $z = 8$, the He II λ1640 line is redshifted to $\lambda = 1.48\,\mu$m, placing it within the *F150W* band for slitless spectroscopic observations with NIRISS. For Pop III.1, the He II λ1640 flux is comparable to that of Hβ. Furthermore, NIRISS *F150W* and NIRCam *F444W* are also comparable in sensitivity. Hence, the integration time of 55.25 h is roughly similar to that of Hβ (17.12 h). However, with Pop III.2 and Pop III Kroupa, the He II line begins to drop off with respect to Hβ and the integration times become much longer, at $\sim$1000 and $\sim$100 000 h, respectively. Thus, a He II λ1640 line detection with NIRISS will only be possible for Pop III.2 sources that are much more massive than the nominal stellar mass ($M_* \sim 5 \times 10^6\,M_\odot$) and/or have been strongly gravitationally lensed ($\mu \sim 5$).

As has been discussed in the literature (see e.g. Schaerer 2002, 2003; Raiter et al. 2010; Grisdale et al. 2021; Nakajima & Maiolino 2022) and will also be discussed more thoroughly in Section 4, the main merit for detecting He II λ1640 is that it is a clear Pop III signature. Although AGN and/or DCBH can also produce bright He II emission (see e.g. Nakajima & Maiolino 2022), these can be readily ruled out from photometry due to their much redder colours (see e.g. Inayoshi et al. 2022, or Fig. A1). Furthermore, a measurement of the He II equivalent width can also distinguish between different Pop III IMFs, and thus (in principle, though in practice can be difficult due to model uncertainties) is able to firmly separate Pop III.1, Pop III.2, and Pop III Kroupa galaxies.

4 POP III CONSTRAINTS FROM FOLLOW-UP SPECTROSCOPY

Having identified potential Pop III candidates either from colour selection, emission-line selection, and/or SED fitting (not covered in this work), deep follow-up spectroscopy will be essential to place tighter constraints on the Pop III nature of these sources. In this section, we outline the NIRSpec spectroscopic observations that could be undertaken, as well as the spectroscopic diagnostics that need to be applied to achieve this. Our emphasis will be on emission line equivalent widths, emission line mass-to-light ratios, and line ratios. We will focus on the brightest lines that will be accessible by NIRSpec that are most sensitive to Pop III star formation. As discussed earlier, at $z = 8$ these lines are Hβ, Lyα, and He II λ1640.

We show the expected emission line fluxes for $z = 8$ Pop III galaxies with $\log(M_*/M_\odot) = 6$ immediately after an instantaneous starburst in Table 4. We also show the expected integration times needed to achieve a 5σ detection of these lines, assuming that the $R = 1000$ NIRSpec gratings (which are the most sensitive gratings for emission line detection) have been used. For Hβ, Lyα, and He II λ1640, this corresponds to the G395M, G140M, and G140M gratings, respectively. We use the *JWST* ETC to perform these integration time estimations, assuming a point source, with a continuum-subtracted spectrum with a five spectral pixel, and four spatial pixel extraction window.

4.1 Hβ diagnostics

4.1.1 Hβ equivalent width

In Fig. 9, we show how the Hβ rest-frame equivalent widths (left-hand panel) and the Hβ line luminosity (right) vary with time after an instantaneous starburst. We again assume a nominal stellar mass of $\log(M_*/M_\odot) = 6$. Hence, the Hβ line luminosity in the right-hand panel is essentially a mass-to-light ratio, representing how much line

Table 4. Similar to Table 3, but now showing the integration times needed to achieve a 5σ line detection with NIRSpec $R \sim 1000$ observations. We estimated the integration times using the *JWST* ETC, assuming a point source, with a continuum-subtracted spectrum with a five spectral pixel, and four spatial pixel extraction window.

IMF	Hβ flux (cgs)	Hβ 5σ exposure time (h)	Lyα flux (cgs)	Lyα 5σ exposure time (h)	He II λ1640 flux (cgs)	He II λ1640 5σ exposure time (h)
Pop III.1	6.76×10^{-19}	1.02	3.31×10^{-17}	0.0059	8.71×10^{-19}	4.76
Pop III.2	2.34×10^{-19}	8.50	1.10×10^{-17}	0.0537	1.58×10^{-19}	144.51
Pop III Kroupa	3.63×10^{-20}	353.06	1.78×10^{-18}	2.05	1.58×10^{-20}	14451.46

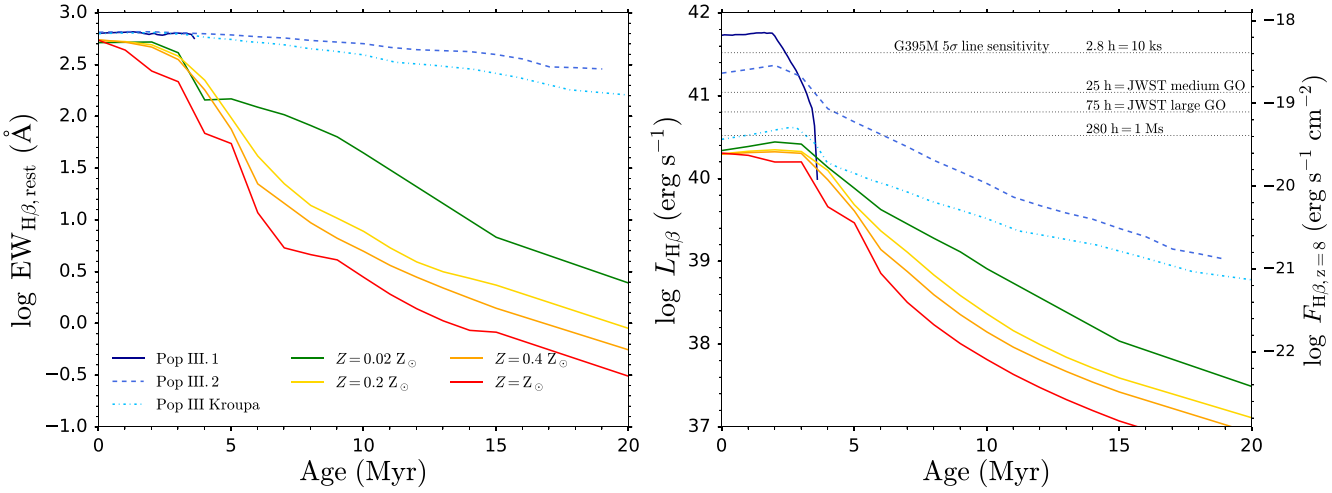

Figure 9. The Hβ rest-frame equivalent width (left-hand panel) and Hβ luminosity (as well as $z = 8$ Hβ flux, right-hand panel) for galaxies at a nominal stellar mass of $\log(M_*/M_\odot) = 6$. The ages refer to the time elapsed after the instantaneous starburst. The dotted horizontal lines in the right-hand panel are the expected 5σ line sensitivities achieved with NIRSpec/G395M (which covers Hβ at $z = 8$) in integration times of 2.8 h = 10 ks, 25 h = *JWST* medium GO program, 75 h = *JWST* large GO program and 280 h = 1 Ms. The colour coding and line styles follow the format of Fig. 3. The Hβ equivalent widths of Pop III galaxies are only marginally higher ($\sim$0.1 dex) than for non-Pop III galaxies. The substantially larger ($\sim$1 dex) Hβ luminosities per unit stellar mass for Pop III galaxies likely cannot be used as a Pop III indicator, as that would require an accurate measurement of the stellar mass, which in turn would require one to already know if the source is Pop III.

luminosity is expected per 10^6 M$_\odot$ formed. As pointed out earlier in this paper, Pop III galaxies have much greater Hβ line luminosities per unit stellar mass formed. However, their continuum normalization per unit stellar mass formed (not shown) is also substantially higher. As a result, their Hβ equivalent widths are only marginally higher ($\sim$0.1 dex) than for non-Pop III galaxies.

In principle, a measurement of the Hβ equivalent width can therefore be used to distinguish between Pop III and non-Pop III galaxies. With a 5σ Hβ detection, the uncertainty on the measured flux will be 20 per cent. However, the separation between Pop III and non-Pop III is $\sim$0.1 dex $\approx$ 25 per cent. Hence, in practice, barring any model uncertainties, a much deeper integration (e.g. 4 $\times$ the integration time) with Hβ detected at 10σ will likely be required to more definitively identify a source as likely being a Pop III galaxy. Given the relatively short exposure times needed to detect Hβ at 5σ with NIRSpec/G395M, at 1.02 and 8.50 h for Pop III.1 and Pop III.2 galaxies, respectively, such deep integrations would certainly be possible to achieve even within a small-to-medium *JWST* GO observing program.

However, there are other complications with using the measured Hβ equivalent width as a Pop III indicator. First, the exact EW associated with Pop III will likely be model dependent, with different models likely predicting different Hβ line luminosities and continuum levels. Indeed, in the Nakajima & Maiolino (2022) models (not shown) the expected Hβ EWs for Pop III galaxies are log EW = 2.95–3.00, whereas for non-Pop III the range is log EW $\leq$ 2.85, thus overlapping with the predicted Pop III EWs in the Zackrisson et al. (2011) models (log EW $\approx$ 2.85).

Secondly, the Hβ EW also depends on the covering fraction f_{cov} of the ISM gas (see e.g. Zackrisson, Inoue & Jensen 2013). The lower the covering fraction, the lower the Hβ line luminosity but also the lower the nebular continuum. Hence, in principle, one would also need to carefully take into account the f_{cov} (or f_{esc}) dependence of the Hβ EW (for more details see Zackrisson et al. 2013) before conclusive inferences on the Pop III nature of the source can be made.

It should be noted that the EWs shown in Fig. 9 correspond to a single stellar population all formed after an instantaneous starburst. For non-Pop III galaxies, there may be an underlying older stellar population, in addition to the newly formed starburst. Provided that this older stellar population provides a non-negligible flux density to the continuum, the observed EWs for non-Pop III galaxies will actually be lower than those shown in Fig. 9.

Furthermore, determining the Hβ EW requires both the Hβ line flux and the continuum level to be measured. As Pop III galaxies are typically very faint (see Fig. 1 and Table 1), detecting their continuum through, e.g. $R \sim$100 NIRSpec/PRISM spectroscopy will be a challenging endeavour (requiring $\sim$28.5–30.5 AB mag depth, barring any flux boost from gravitational lensing or elevated Pop III stellar masses). Therefore, the continuum flux density of

Pop III galaxies will likely have to be estimated from broad-band photometry. However, the difficulty with this is that the bandpass-averaged flux densities measured via photometry can be strongly boosted (by e.g. >0.1 dex = 0.25 mag) above the continuum level by the high EW emission lines in Pop III galaxies (as shown in Fig. 1). This makes estimating the true continuum level around Hβ particularly difficult as it itself has a high EW and it is also bracketed by a series of bright emission lines at shorter (e.g. Hγ) and longer wavelengths (e.g. Hα). In principle, this flux boost effect can be corrected for by taking into account the measured Hβ flux (and all other high EW lines that reside within the filter of interest), as the observed bandpass-averaged flux density $f_{\lambda,\,\mathrm{obs}} = f_{\lambda,\,\mathrm{cont}} + f_{\mathrm{lines}}/\Delta\lambda$, where $f_{\lambda,\,\mathrm{cont}}$ is the true continuum level, f_{lines} is the total flux of all the emission lines that reside within the filter, and $\Delta\lambda$ is the bandpass width of the filter. Thus, the potential difficulty in accurately estimating the continuum flux density (and the measurement error on the Hβ flux), together with the small difference in Hβ EW between Pop III and non-Pop III (and systematics and secondary dependences therein), likely renders the Hβ EW impractical as a diagnostic for actually distinguishing between Pop III and non-Pop III galaxies.

4.1.2 Hβ luminosity

As can be seen from Fig. 9, the Hβ luminosity starts to drop off substantially ∼3 Myr after an instantaneous starburst. Thus, the visibility window over which the Hβ emission from Pop III galaxies can likely be detected with *JWST* (∼3 Myr) is comparable to the time-scale over which these galaxies can be detected in broad-band photometry (2.8–5.6 Myr, see Table 1). Note that the Hβ luminosities (and fluxes) shown in Fig. 9 are for galaxies at a fixed stellar mass $M_* = 10^6\,\mathrm{M}_\odot$, and hence can be taken as an indication of the Hβ luminosity per unit stellar mass ($=L_{\mathrm{H}\beta}/10^6$).

Now, given the large separation in Hβ luminosity per unit stellar mass between Pop III and non-Pop III (∼1 dex), as well as the various Pop III IMFs (∼0.5 dex between Pop III.1 and Pop III.2), an accurate measurement of the line luminosity per unit stellar mass would enable one to readily confirm the Pop III nature of a source. Whilst the determination of the line luminosity is relatively straightforward, the difficulty lies in establishing the stellar mass. Indeed, the continuum flux density per unit stellar mass is vastly different for Pop III and non-Pop III galaxies (not shown), i.e. Pop III galaxies have much lower mass-to-light ratios. This can be inferred from considering the fact that the Hβ line luminosities are much greater for Pop III, while their Hβ EWs are almost the same as non-Pop III. As a result, an accurate determination of the stellar mass therefore requires an accurate assessment of the mass-to-light ratio. However, accurately knowing the mass-to-light ratio is akin to knowing whether the source is Pop III or not (as the M/L ratio is much lower for Pop III). Thus, in order to determine whether a source is Pop III from its line luminosity per unit stellar mass, we would have to already know if it was Pop III or not, making this diagnostic unusable in practice.

4.2 Lyα diagnostics

We show the *intrinsic* Lyα rest-frame equivalent widths and line luminosities in Fig. 10. As alluded to earlier, unlike the Balmer recombination lines, the Lyα EW is much larger for Pop III galaxies relative to non-Pop III. Thus, a measurement of the *intrinsic* Lyα EW would not only enable one to readily separate Pop III from non-Pop III, but in principle it would also enable one to distinguish between different Pop III IMFs.

However, in practice, the Lyα line will likely be heavily attenuated and scattered by the IGM. Hence, the *observed* Lyα line luminosities and EWs will likely be substantially lower than those shown in Fig. 10, which would erode this otherwise strong Pop III signature.

4.3 He II λ1640 diagnostics

4.3.1 He II λ1640 equivalent width

We show the He II λ1640 rest-frame equivalent width, line luminosity and flux ratio with Hβ in Fig. 11. We see that bright He II λ1640 emission is a clear spectroscopic signature for Pop III galaxies (as has been previously suggested in e.g. Schaerer 2002, 2003; Raiter et al. 2010; Grisdale et al. 2021; Nakajima & Maiolino 2022), as they have substantially higher EWs than non-Pop III. Hence, a measurement of the EW will establish the Pop III nature of a source. Furthermore, the various Pop III IMFs also yield distinctly different He II λ1640 EWs (with a ∼0.5 dex spread).

Using the Nakajima & Maiolino (2022) Pop III models (not shown here but see their Fig. 6), we have investigated the dependence of the He II λ1640 EW on ionization parameter U, finding only a very weakly decreasing trend (with $\Delta\log\mathrm{EW} \approx 0.07$ dex) with increasing U (from $U = -2.0$ to -0.5). Thus, the EW ranges spanned by each IMF is distinct, even within the range of possible U values. However, the He II λ1640 EWs do depend somewhat on the covering fraction f_{cov}, with $\Delta\log\mathrm{EW} \approx 0.1$ dex between $f_{\mathrm{cov}} = 0.5$, 1. We note that while the dependence of the He II λ1640 EW on ionization parameter U is relatively weak in the Nakajima & Maiolino (2022) models (over the range $-2.0 < U < -0.5$, it is much stronger (≥0.2 dex) in the models of Raiter et al. (2010) (over the range $-4.0 < U < -1.0$ with $n_{\mathrm{H}} = 10^3\,\mathrm{cm}^{-3}$). However, most of this ionization parameter dependence stems from the evolution between $-4 < U < -2$, with only weak trends in the range $-2 < U < -1$, similar to the Nakajima & Maiolino (2022) models.

Furthermore, we note that while models generally predict Pop III galaxies to have characteristically high He II λ1640 EWs (compared to non-Pop III galaxies), with the EW tending to increase as the IMF becomes increasingly top-heavy, there is some variation in the actual EW predicted by the different models, which could render a determination of the Pop III IMF difficult. In the Zackrisson models shown in Fig. 11, the predicted Pop III He II λ1640 rest-frame EWs are in the range 16–50 Å, while for the Nakajima & Maiolino (2022) models the range is instead 25–80 Å, with Raiter et al. (2010) and Inoue (2011) predicting 20–90 and 15 Å, respectively. Despite the aforementioned secondary dependences and systematics, a measurement of the He II λ1640 EW should help to place valuable constraints on the Pop III IMF.

Now, determining the He II λ1640 EW also requires the continuum level to be estimated (which is likely more viable via broad-band photometry, rather than spectroscopy, as 28.5–29.5 AB mag depth is required). In contrast to Hβ, the EW of He II λ1640 is relatively small and the spectrum around 1640 Å is relatively devoid of bright emission lines (with the exception of Lyα, see Fig. 1). Hence the true continuum level around He II λ1640 can be relatively well estimated from broad-band photometry (using e.g. the *F150W* or *F200W* filters at $z = 8$). However, given the narrow width of the NIRSpec slits (0.2 arcsec), the physical scale associated with the He II λ1640 emission (probed with NIRSpec) may be different to the physical scale associated with the broad-band continuum emission (probed by NIRCam). Thus, it may in principle be difficult to accurately determine the He II λ1640 EW from a combination of NIRSpec and NIRCam data. While this potential issue should not matter for

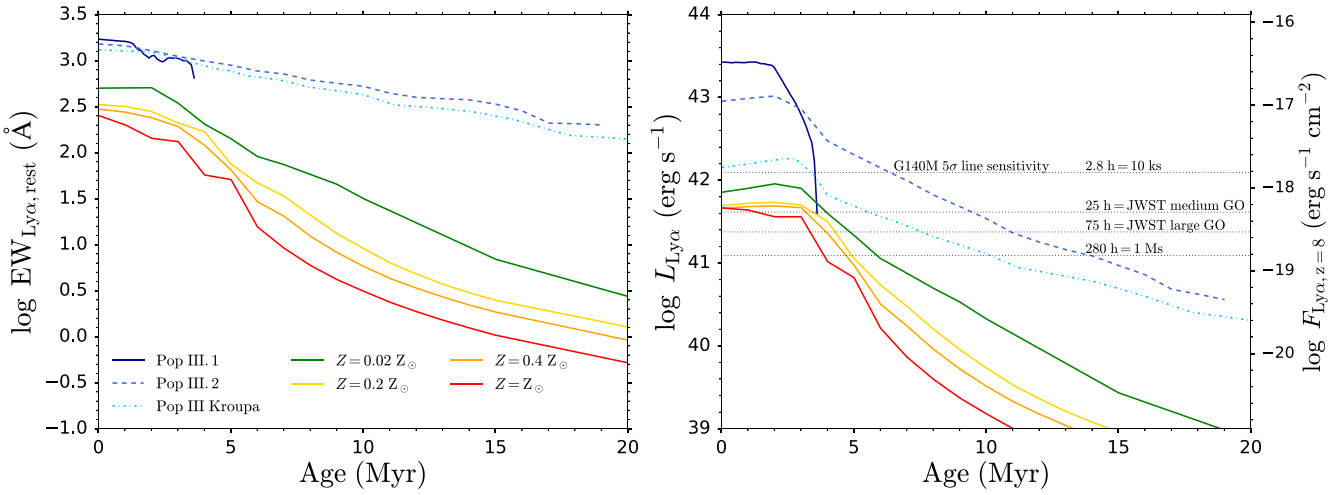

Figure 10. Similar to Fig. 9, but now showing Lyα. Note that we show the *intrinsic* (i.e. not attenuated by the IGM) Lyα EW and luminosity. In practice, the Lyα line will likely be heavily attenuated/scattered by the IGM, both blueward and redward of the line centre. The dotted horizontal lines in the right-hand panel are now the expected 5σ line sensitivities achieved with NIRSpec/G140M (which covers Lyα at $z = 8$).

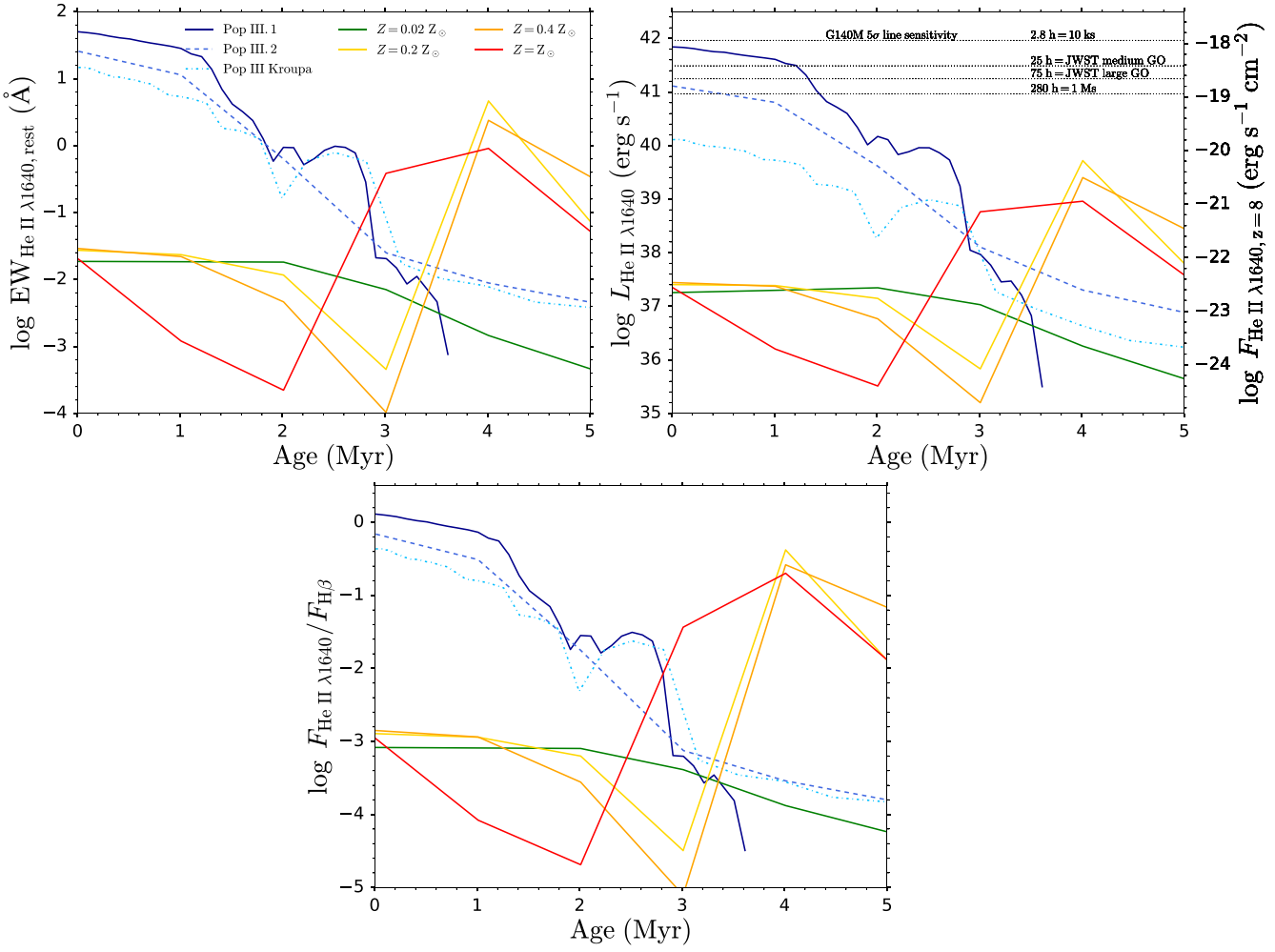

Figure 11. Similar to Fig. 9, but now showing He II λ1640. The dotted horizontal lines in the top right-hand panel are now the expected 5σ line sensitivities achieved with NIRSpec/G140M (which covers He II λ1640 at $z = 8$). We also show the He II λ1640/Hβ line ratio (bottom panel). Note that the ages are only shown up to 5 Myr, rather than 20 Myr as in Fig. 9. High EW He II λ1640 emission will serve as the definitive indicator of Pop III galaxies.

distinguishing between Pop III and non-Pop III galaxies (due to their very large separation in He II λ1640 EW), it may complicate the determination of the Pop III IMF. Nevertheless, provided that Pop III galaxies are very compact/point-sources (which seems reasonable to assume), then the He II λ1640 EW and thus the Pop III IMF should be able to be determined relatively accurately.

4.3.2 *He II λ1640/Hβ ratio*

We also show the He II λ1640/Hβ ratio in Fig. 11, where there is a ∼0.5 dex spread between the different Pop III IMFs. The benefits for considering this ratio in Pop III searches are twofold.

First, in the case of both a He II λ1640 and Hβ detection, the line ratio can be computed. This ratio is less sensitive to the ionization parameter U than the He II λ1640 EW, with $\Delta \log \mathrm{EW} \approx 0.02$ dex from $U = -2.0$ to -0.5. The dependence on f_{cov} is similar, with $\Delta \log \mathrm{EW} \approx 0.1$ dex between $f_{\mathrm{cov}} = 0.5, 1$. Thus, a measurement of the He II λ1640/Hβ ratio would therefore in principle enable tighter constraints on the Pop III IMF.

Secondly, although the He II λ1640 line is comparable in brightness to Hβ for the Pop III.1 and Pop III.2 IMFs (see Table 4), it resides in the G140M NIRSpec grating at $z = 8$. This grating is roughly 3 × less sensitive than the G395M grating which covers Hβ. Hence, the integration times needed to detect He II λ1640 at 5σ are roughly 5–15 × longer than those needed to detect Hβ at 5σ. Indeed the integration times needed to detect He II λ1640 at 5σ will require medium-deep to ultra-deep integrations, with 4.76 to 144.51 h needed for Pop III.1 and Pop III.2, respectively (assuming $M_* = 10^6\,\mathrm{M}_\odot$). Thus, in many cases, only Hβ will be detected with *JWST*. Nevertheless, a He II λ1640 non-detection can still be used to place valuable upper limits on the Pop III IMF, as from the non-detection one can begin to rule out the more top heavy IMFs. Of course, if the source is reasonably magnified ($\mu \approx 2$–3), or is some small multiple of the nominal stellar mass, then even for the Pop III.2 IMF a line detection can be made within a medium *JWST* GO program (25–75 h).

4.3.3 *He II λ1640 luminosity*

We note that the He II λ1640 luminosity for Pop III galaxies begins decreasing immediately after an instantaneous starburst, with an even steeper decline after 1–1.5 Myr. Thus, the visibility window over which the He II λ1640 emission from Pop III galaxies can be detected with *JWST* (∼1–1.5 Myr) is even shorter than the visibility windows for Hβ and Lyα detections (3 Myr) and detections in broad-band photometry (2.8–5.6 Myr). Thus, even if a true Pop III galaxy has been identified as a Pop III candidate from photometry, there is no guarantee that its Pop III nature can be definitively established from deep follow-up spectroscopy. As if the galaxy is observed too late after the initial starburst, its He II λ1640 emission will likely be too faint to detect, with the inferred He II λ1640 EW therefore being too low for the galaxy to be classified as Pop III.

4.4 He II λ4686

The He II λ4686 recombination line is also accessible with NIRSpec. In principle, this line could also be used as a spectroscopic Pop III indicator. Indeed, He II λ4686 resides in the 3 × more sensitive G395M grating, together with Hβ. However, the He II λ4686 line is roughly an order of magnitude fainter than He II λ1640 (in the Zackrisson et al. 2011 Pop III models, but see also Osterbrock & Ferland 2006). Hence, a 5σ line detection would take approximately 10 × longer than for He II λ1640 and roughly 100 × longer than for Hβ, thereby making it impractical to use this line as a Pop III indicator.

4.5 Metallicity constraints from [O III] non-detections

At $z = 8$ the [O III] λ5007 line is also redshifted into the G395M grating, similar to Hβ. Conveniently, the [O II] λλ3726, 3729 doublet also falls within the G395M grating at these redshifts. At intermediate-to-high metallicities and ionization parameters, the [O III] λ5007 line is brighter than Hβ. Hence, a Hβ detection (at e.g. 5σ), together with a [O III] λ5007 non-detection, can place valuable upper limits on the metallicity of a galaxy.

In Fig. 12, we show the [O III] λ5007/Hβ line ratio (left-hand panel) and the [O II]/Hβ line ratio (right-hand panel) for the Nakajima & Maiolino (2022) models. We have chosen to use the Nakajima & Maiolino (2022) models for this analysis because they enable one to explore the dependence of the line ratios on ionization parameter U, and also because they extend down to lower metallicities. We find that at most metallicity and ionization parameter combinations the [O III] λ5007 line is brighter than Hβ. Hence, in this regime, the [O III] λ5007 line should be detected if Hβ has been detected. It is only at low ionization parameter that [O III] λ5007 begins to become fainter than Hβ, and we may expect a [O III] non-detection. However, it is precisely at these low ionization parameters that the [O II] line becomes brighter than Hβ. Hence, there is a sort of 'see-saw effect', where one of [O III] or [O II] is always brighter than Hβ (assuming no dust attenuation dimming the [O II] doublet) across the range of possible ionization parameters. Hence, if both [O III] λ5007 and [O II] are not detected, but Hβ is detected, then the metallicity of the galaxy is likely below $Z = 0.1\,Z_\odot$.

Pushing to even lower metallicities, we now turn to Fig. 13. We show the [O III] λ5007/Hβ ratios for the Nakajima & Maiolino (2022) and Zackrisson et al. (2011) models in the left-hand and right-hand panels, respectively. We see that for the Zackrisson et al. (2011) models (which adopt a spherical geometry for the H II region and therefore a radially varying ionization parameter for each metallicity), the [O III] λ5007 line is brighter than Hβ even at $Z = 0.02\,Z_\odot$, provided that we see the galaxy within ∼5.5 Myr after the starburst. We note that it is unlikely for non-Pop III galaxies to be mistakenly identified as Pop III candidates ≥5 Myr after a starburst, as demonstrated by our colour selections in Section 3.2, hence the weaker [O III] λ5007 emission in this regime is likely not a concern. If the radially-varying ionization parameters in the Zackrisson et al. (2011) models are representative of the ionization parameters we expect to find in galaxies at $z \sim 8$, then a Hβ detection, together with an [O III] λ5007 non-detection, implies that the metallicity is likely below $Z = 0.02\,Z_\odot$.

Now, if we consider the Nakajima & Maiolino (2022) models in the left-hand panel, we find that the [O III] λ5007 line begins to dip below Hβ in brightness at $Z = Z_\odot/140$. Indeed, at $\log U = -2.0$, we find that the logarithm of the [O III] λ5007/Hβ ratio is −0.5. Therefore, if Hβ is detected at 5σ in this scenario, a 10 × longer integration time would be needed to detect [O III] λ5007 (at 5σ). In other words, once Hβ is detected, a 10 × longer integration time is needed to establish that the metallicity is $Z \leq Z_\odot/140$.

If such a deep integration in the G395M grating is considered, it is likely better placed to instead opt for an equally deep integration in the G140M grating instead. As discussed in Section 4.3 and shown in Table 4, one requires a roughly 5–15 × longer integration to detect He II λ1640 compared to Hβ. A He II λ1640 line detection would

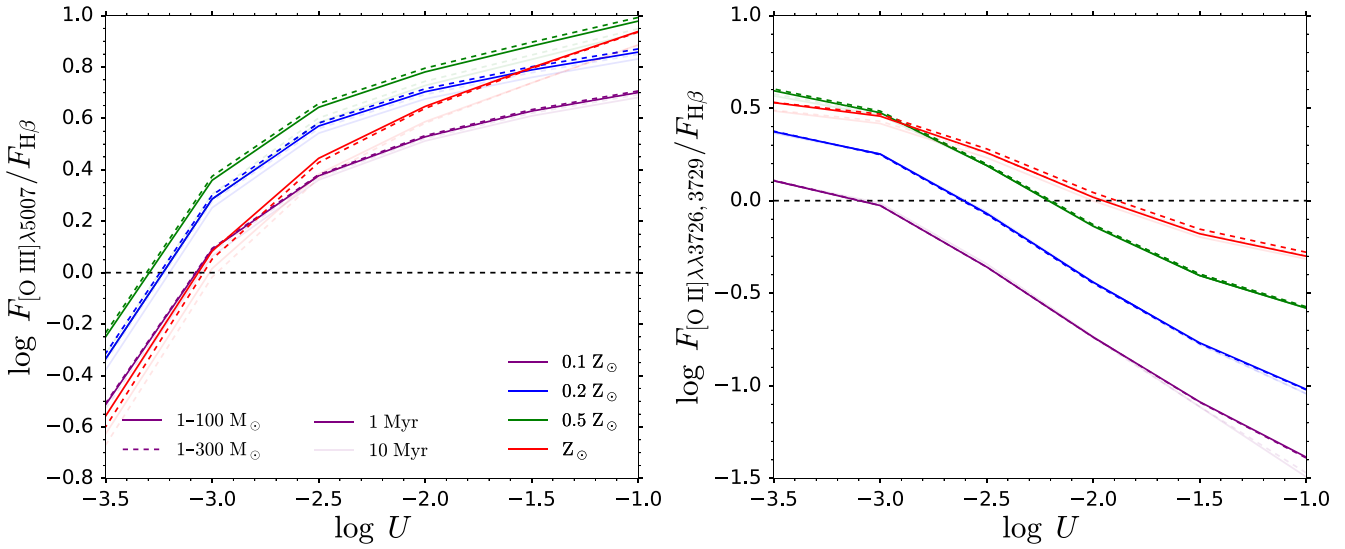

Figure 12. The [O III] λ5007/Hβ line ratio (left-hand panel) and [O II] λλ3726, 3729/Hβ ratio (right), as a function of ionization parameter U using the Nakajima & Maiolino (2022) models. We show the line ratios for metal-rich Pop I galaxies at metallicities $Z = 0.1\,Z_\odot$ (purple), $Z = 0.2\,Z_\odot$ (blue), $Z = 0.5\,Z_\odot$ (green), $Z = Z_\odot$ (red), adopting a Kroupa (2001) IMF with upper mass limits of 100 $M_\odot$ (solid) and 300 $M_\odot$ (dashed), at 1 Myr (unfaded) and 10 Myr (faded) after the starburst. At these high metallicities, always one of [O III] λ5007 or [O II] is brighter than Hβ (assuming no dust attenuation dimming the [O II] doublet). Hence, if both [O III] λ5007 and [O II] are non-detected, but Hβ is detected, then the metallicity of the galaxy is likely below $Z = 0.1\,Z_\odot$.

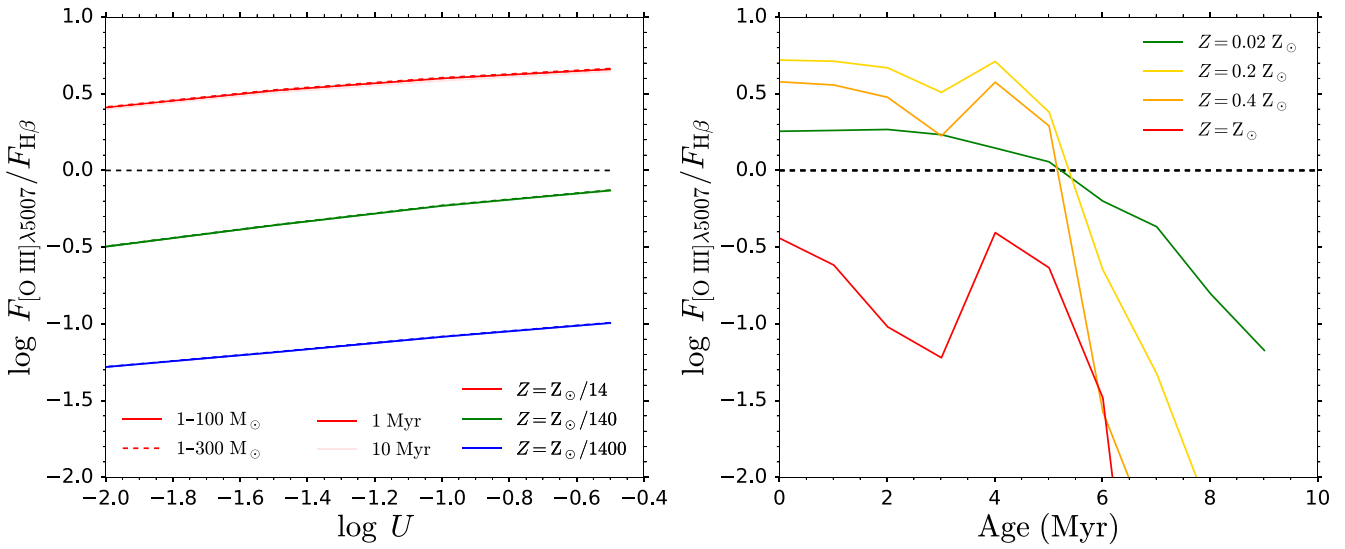

Figure 13. The [O III] λ5007/Hβ line ratio for metal-poor Pop II galaxies using the Nakajima & Maiolino (2022) models (left-hand panel) at metallicities $Z = Z_\odot/14$ (red), $Z = Z_\odot/140$ (green), and $Z = Z_\odot/1400$ (blue). The line ratios for the non-Pop III Zackrisson et al. (2011) models (right), following the colour coding of Fig. 3. In the Zackrisson et al. (2011) models, [O III] λ5007 is brighter than Hβ even at $Z = 0.02\,Z_\odot$. In the Nakajima & Maiolino (2022) models, [O III] λ5007 begins to become fainter than Hβ at $Z = Z_\odot/140$. Hence, a Hβ detection, together with an [O III] λ5007 non-detection, implies that the metallicity is likely below $Z = 0.02\,Z_\odot$. A 10 × longer integration time than was needed to detect Hβ is needed to establish that the metallicity is $Z \leq Z_\odot/140$.

yield much more conclusive constraints on both the Pop III nature of a source and the Pop III IMF, than can possibly be inferred from upper limits on the metallicity from non-detections of [O III] λ5007.

4.6 Hα versus Hβ at $z = 8$

Our discussion of Balmer recombination lines has thus far centred around Hβ for it lies within the NIRSpec spectral range at $z = 8$. In contrast, the intrinsically brighter Hα line is redshifted into the MIRI/MRS spectral range at this redshift. Although Hα is roughly 3 × brighter than Hβ (barring any dust, which seems reasonable to ignore for pristine Pop III galaxies, see e.g. Zackrisson et al. 2011), MIRI is roughly 6 × less sensitive (at the Hα wavelength) than NIRSpec (at the Hβ wavelength). Hence, the integration time needed for a 5σ detection of Hα at $z = 8$ will be roughly 4 × longer than that needed for Hβ. Furthermore, while there are additional merits to observing Hβ due to added metallicity constraints from [O III] non-detections (a line that is typically *brighter* than Hβ), non-detections of the neighbouring [N II] and [S II] doublets around Hα yield no such constraints as these lines are typically *fainter* than Hα

(see e.g. Baldwin, Phillips & Terlevich 1981; Kewley et al. 2001; Steidel et al. 2014; Shapley et al. 2015; Curti et al. 2022).

4.7 Metal line (non-)detections with ALMA

In the epoch of reionization, [O III] 88 μm is likely the brightest emission line in the rest-frame FIR, usually being brighter than [C II] 158 μm (see e.g. Laporte et al. 2019; Harikane et al. 2020; Katz et al. 2022). Here, we briefly discuss the merits for following-up potential Pop III candidates with ALMA to rule out metal-line emission and hence place constraints on the metallicity. Depending on the ISM temperature, the [O III] λ5007 line is between 1–10 × more luminous than [O III] 88 μm (see e.g. Moriwaki et al. 2018; Yang & Lidz 2020). Furthermore, NIRSpec/G395M is roughly 2 × more sensitive than ALMA at emission line detection. Hence, the integration times needed to detect [O III] 88 μm with ALMA are 4–400 × longer than what is needed to detect [O III] λ5007 with *JWST*. Thus, NIRSpec is currently the optimal instrument for spectroscopic follow-up of potential Pop III candidates.

4.8 Spectroscopic follow-up with 25 + m telescopes

The next generation of 25 + m class, extremely large telescopes will likely play a complementary, synergistic role with *JWST*. Indeed, with their ∼5 × wider mirror diameters, they will have both a vastly larger light collecting area, as well as significantly less light smearing (by diffraction, provided that adaptive optics is used). This makes such telescopes ideal for deep follow-up spectroscopic observations of potential Pop III candidates identified by *JWST*. Indeed, provided that the emission line of interest does not sit on top of a skyline, these 25 + m telescopes will be substantially more sensitive at emission line detection than *JWST*.

At $8 \leq z \leq 10$, the He II λ1640 line is redshifted into the *H*-band of TMT/IRMS, the planned infrared multi-object spectrograph for the Thirty Meter Telescope. Assuming a point source (which seems reasonable for a Pop III galaxy), the expected emission-line sensitivity in the *H*-band is 5.6×10^{-19} erg s^{-1} cm^{-2} at 10σ within a 1 h integration (Skidmore 2015). Similarly, ELT/MOSAIC, the infrared multi-object spectrograph for the upcoming Extremely Large Telescope, is expected to have an emission-line sensitivity of 6.3×10^{-19} erg s^{-1} cm^{-2} (Evans et al. 2015). Thus, these next-generation ground-based spectrographs will be roughly an order of magnitude more sensitive than NIRSpec/G140M, which has a sensitivity of 3.8×10^{-18} erg s^{-1} cm^{-2}. Hence, the integration times needed to achieve a line detection of He II λ1640 with 25 + m telescopes will essentially be ≈100 × shorter than the integration times needed with *JWST*. Thus, such telescopes should readily be able to spectroscopically follow-up potential Pop III candidates (identified through *JWST* NIRCam + MIRI photometry and/or slitless spectroscopy) and confirm their Pop III nature through a detection of the He II λ1640 line (for more details, see Grisdale et al. 2021), requiring roughly only 0.05 and 1.45 h of integration for the Pop III.1 and Pop III.2 IMFs, assuming a $M_* = 10^6$ M$_\odot$ Pop III galaxy. For lower mass Pop III galaxies, such as those residing in minihalos with $M_* = 10^{2-3}$ M$_\odot$, even more sensitive instrumentation will be needed, such as the potential Moon-based 100-m Ultimately Large Telescope discussed in Schauer, Drory & Bromm (2020).

Ultimately to find Pop III galaxies, we will need to use a combination of photometry to find good candidates and then spectroscopy to follow them up and ensure that no metal lines are present. However, with the large number of distant galaxies that *JWST* is finding, and will continue to find, a photometric method for selecting candidates, such as what we present here, is necessary to remove systems that have properties that are not consistent with being Pop III galaxies.

5 ON THE STELLAR MASSES, REDSHIFTS AND LIKELIHOOD OF ENCOUNTERING POP III GALAXIES

In this section, we briefly discuss our assumptions regarding the stellar masses of Pop III galaxies, their redshifts and the general likelihood of encountering Pop III galaxies with *JWST*.

Throughout this paper, we have assumed a nominal Pop III stellar mass of $M_* = 10^6$ M$_\odot$. We have adopted this stellar mass not because it is realistic (as theory/simulations generally expect lower Pop III masses), but rather because it is practical, likely representing the least massive Pop III galaxies that can be detected with *JWST* (without gravitational lensing). Indeed, as has already been discussed in the introduction, based off of simple virial arguments for an atomic cooling halo, one might expect a typical Pop III stellar mass of $M_* = 10^5$ M$_\odot$. Depending on the assumed star formation efficiency, and as shown in e.g. semi-analytic models of Pop III star formation (see e.g. Hartwig et al. 2018, 2022), the typical total mass of Pop III stars formed may be $M_* = 10^4$ M$_\odot$ or lower. Moreover, this Pop III star formation likely proceeds over some small (but finite) timescale, rather than the instantaneous Pop III starburst we assume in our analysis. This non-instantaneous Pop III star formation timescale can be important when it comes to the observability of Pop III galaxies, due to the short window over which the continuum emission (2.8–5.6 Myr) and line emission (1–1.5 Myr for He II λ1640) can be detected, even for an instantaneous starburst. Thus, the massive ($M_* = 10^6$ M$_\odot$), instantaneous starburst Pop III galaxies we assume in this work may be very rare (though see also Inayoshi, Li & Haiman 2018). Now, for each order of magnitude decrease in Pop III stellar mass, the required integration times will increase by 100× the tabulated values in Tables 1–4. Hence, as has been discussed earlier, strong gravitational lensing will be essential to detect these lower mass Pop III galaxies, likely requiring larger magnifications than the $\mu = 2$–3 we typically assume in this work. Indeed, the magnification factors for compact objects (like Pop III galaxies) can indeed be very high (though rare, see e.g. Zackrisson et al. 2012; Zackrisson et al. 2015; Windhorst et al. 2018), with for example magnifications of $\mu = 30$–70 having been observed for young massive star clusters of $M_* \sim 10^{6-7}$ M$_\odot$ and with effective radii $R_e \sim 1$–20 pc in the $z \sim 6$ Sunrise arc (Vanzella et al. 2023). Thus, although such lower stellar mass Pop III galaxies may be more realistic (and hence more abundant), the steep gravitational lensing requirement (and rarity thereof) will likely still make it challenging to encounter (and detect) such systems with *JWST*.

With regards to the redshifts of these Pop III galaxies, we have based our colour selections (in the main body of the paper) around a nominal redshift of $z \sim 8$ (this is extended to $z \sim 10$ in Appendix B). This redshift was adopted, again, not because it is the most realistic redshift to find Pop III galaxies (as the Universe is more chemically pristine at even higher redshifts), but rather because it is practical, being roughly the highest redshift at which some key Pop III tracers are still accessible by NIRCam/NIRSpec, which allows for a much more efficient identification and spectroscopic follow-up of Pop III candidates. Indeed, above this redshift, the lack of metal-line emission (traced by [O III] λ5007), as well as the (marginally) stronger Hβ emission, are redshifted into the MIRI regime, with both the MIRI imager and spectrograph being >7 × less sensitive than their NIRCam/NIRSpec counterparts (thus requiring >50 × the

integration time) and having a smaller imaging footprint (4 × smaller, 2.35 versus 9.7 arcmin^2) and lack of spectroscopic multiplexing (1 object versus dozens of galaxies). Of course, the greater the redshift of the galaxy, roughly the greater the likelihood of it being Pop III, simply due to the Universe still being relatively chemically pristine due to a lack of enrichment by prior star formation. Indeed, according to the simulations in Pallottini et al. (2014), the mean baryon metallicity is $Z = 10^{-3.75}\,Z_\odot$ at $z = 8$, while only being $Z = 10^{-4.75}\,Z_\odot$ at $z = 10$, with $Z_{\rm crit} = 10^{-4}\,Z_\odot$ commonly being assumed to be the critical metallicity marking the transition point between Pop III and Pop II star formation.

Finally, we also assume that our Pop III galaxies are purely composed of Pop III stars. Of course, galaxies with a mixture of Pop III and chemically-enriched Pop II stars are also possible (see e.g. Sarmento, Scannapieco & Pan 2017; Riaz, Hartwig & Latif 2022; Venditti et al. 2023). Provided that these two stellar populations are spatially separate (as seen through the resolution of *JWST*), it should in principle be possible to disentangle the Pop III component from the metal-enriched components, provided that a spatially resolved analysis is undertaken (and the necessary signal to noise is available), enabling our pure Pop III selections and diagnostics to still be applied. However, if these two populations are mixed (from the observer's perspective), then the Pop II stars will likely erode the characteristic Pop III signatures that we have discussed in this article, with the extent of the erosion depending on the relative brightness (for more details, see e.g. Riaz et al. 2022) of the Pop II stars/gas to the Pop III (and also on the metallicity of the Pop II stars/gas). For example, [O III] and [S III] emission from the Pop II gas will contaminate the pure Pop III emission, causing the galaxy to (begin to) drift out of the Pop III region of the *F444W*−*F560W*, *F560W*−*F770W* colour–colour plane, causing such systems to be potentially missed by our pure Pop III colour selections, depending on the brightness and metallicity of the Pop II stars/gas. Additionally, the additional stellar + nebular continuum, plus the lack of He II λ1640 emission originating from the Pop II stars/gas, can result in a net (Pop III + Pop II) He II λ1640 equivalent width that falls below the expected range for pure Pop III galaxies, again, causing such Pop III + Pop II mixed systems to be missed in our pure Pop III classifications.

With the aforementioned caveats in mind, we now briefly discuss the likelihood of encountering Pop III galaxies with *JWST*. We will adopt three different approaches to estimate the expected number of bright/massive Pop III galaxies on the sky.

First, we use the expected Pop III cosmic star formation rate density, assuming a nominal value of $10^{-4}\,{\rm M}_\odot\,{\rm yr}^{-1}\,{\rm Mpc}^{-3}$ at $z = 8$ and 10 (see e.g. Sarmento, Scannapieco & Cohen 2018). Similar to the rest of our analysis, we make the simplifying assumption that all Pop III galaxies are massive, i.e. with $M_* = 10^6\,{\rm M}_\odot$, and form their stars over a very short/almost instantaneous time-scale, i.e. $\Delta t = 0.1$ Myr (which is comparable to the free-fall time for a gas cloud of the same mass and a radius of 5 pc). Following the methodology in Windhorst et al. (2018), the $10^{-4}\,{\rm M}_\odot\,{\rm yr}^{-1}\,{\rm Mpc}^{-3}$ Pop III cosmic star formation rate density thus translates into a Pop III comoving number density of $n = 10^{-5}\,{\rm Mpc}^{-3}$. This in turn corresponds to an expected number of 0.20 and 0.16 massive Pop III galaxies per NIRCam field of view and per unit redshift interval, at $z = 8$ and 10, respectively, i.e. we expect to detect one massive Pop III galaxy every 5 or 6 NIRCam pointings. Of course, not all Pop III galaxies will be so massive (in fact, we likely expect such systems to be rare, though see Inayoshi et al. 2018 for a formation mechanism for such massive Pop III systems), so the expected number of actual NIRCam pointings needed will likely be much higher (Inayoshi et al. 2018 find this to be ∼30 NIRCam pointings at $z = 15$).

Secondly, we use another result from Sarmento et al. (2018), namely that the expected fraction of Pop III-bright galaxies (i.e. galaxies with at least 75 per cent of their flux coming from Pop III stars, thus akin to the pure Pop III galaxies we assume in this work) is 1 and 5 per cent of all galaxies brighter than $m_{\rm UV} = 31.4$ mag at $z = 8$ and 10, respectively. Using the Adams et al. (2023b) UV luminosity functions, this translates into an expected comoving density of 1.8×10^{-4} and $1.6 \times 10^{-4}\,{\rm Mpc}^{-3}$ Pop III-bright galaxies at $z = 8$ and 10, respectively. In turn, this amounts to 3.6 and 2.7 Pop III-bright galaxies (with $m_{\rm UV} < 31.4$ mag) per NIRCam field of view and per unit redshift interval. As shown in Table 1, ultra-deep (∼100 h) integrations are required to reach such depths (31.4 AB mag) with *JWST*/NIRCam.

Thirdly, we use the result from Stiavelli & Trenti (2010), who find that the expected Pop III galaxy formation rate is $\sim 2 \times 10^{-8}\,{\rm Mpc}^{-3}\,{\rm yr}^{-1}$ at $z = 10$. Following their line of argument, assuming a Pop III visibility time of 2 Myr, this corresponds to an expected Pop III surface density of ∼800 galaxies per NIRCam FoV per unit redshift interval. However, the majority of these objects will likely be too faint to detect (without gravitational lensing), likely being less massive than the nominal $M_* = 10^6\,{\rm M}_\odot$ we assume for detection with *JWST*. Indeed, Stiavelli & Trenti (2010) note that at $z = 10$, an atomic cooling halo (with $T = 10^4$ K) has a halo mass of $\sim 3.7 \times 10^7\,{\rm M}_\odot$ and a baryonic mass of $\sim 6 \times 10^6\,{\rm M}_\odot$, which would therefore require a star formation efficiency $\epsilon = 0.15$ to produce $10^6\,{\rm M}_\odot$ in stars, which they deem unlikely.

For a detailed investigation into the prospects of detecting Pop III galaxies in blind surveys, we refer the reader to Vikaeus et al. (2022). They find that photometric surveys will likely pick up lensed Pop III galaxies if the Pop III star formation efficiencies are sufficiently high ($\epsilon > 0.005$), though this is model-dependent. Moreover, the photometric prospects are better for the *RST* than for *JWST* or *Euclid*. However, simulations predict that the Pop III number densities are likely too low for spectroscopic detection of He II λ1640 for gravitationally lensed Pop III galaxies in wide-area surveys with *JWST*, *RST*, and *Euclid*. Instead, they argue that targeted cluster lensing surveys with *JWST* likely offer the best prospects for spectroscopic detection of Pop III galaxies.

6 SUMMARY AND CONCLUSIONS

In this paper, we investigate the prospects for observing and identifying Pop III galaxies with *JWST*. We based our analysis on two different, but complementary Pop III models: Zackrisson et al. (2011) and Nakajima & Maiolino (2022). The basis for this approach was twofold. First, to establish the robustness of our colour selections and spectroscopic diagnostics in identifying and confirming Pop III candidates. Secondly, to draw upon the synergy between these two different models. With the Zackrisson et al. (2011) models, we are able to determine the expected apparent magnitudes of $z = 8$ Pop III sources in various NIRCam and MIRI filters, as well as the expected line fluxes of the brightest, most sensitive tracers of Pop III stars. On the other hand, with the Nakajima & Maiolino (2022) models, we explore the dependence of emission line diagnostics on the ionization parameter U and push our analysis of non-Pop III galaxies down to even lower (but still non-pristine) metallicities. In the main body of the paper, we concentrated on $z \sim 8$ galaxies, as at these redshifts the Hβ and [O III] λ5007 lines are still accessible with NIRCam and NIRSpec. In the appendix, we undertook a similar analysis for $z \sim 10$ Pop III galaxies. Our main findings at $z \sim 8$ are summarized below.

Assuming a $z = 8$ Pop III galaxy at the nominal stellar mass of $M_* = 10^6\,{\rm M}_\odot$, we find that deep NIRCam imaging (∼28.5–

30.0 AB mag, 1–20 h) and deep-to-ultra-deep MIRI F560W imaging (∼27.5–29.0 AB mag, 10–100 h) will be needed to achieve a 5σ detection, even for the more top-heavy Pop III.1 and Pop III.2 IMFs. Indeed, detections in the MIRI *F770W* band and beyond will likely be very challenging, with the flux boost from either strong gravitational lensing ($\mu = 10$) and/or fortuitous imaging of exceptionally massive ($M_* = 10^7$ M$_\odot$) Pop III galaxies being essential. Hence, deep imaging of lensing clusters and/or deep-and-wide imaging of many fields will likely be needed to find such bright Pop III sources.

We discuss a number of colour–colour selections to identify Pop III galaxy candidates, outlining the physical basis behind the colour selection, the redshift window of applicability and potential Galactic and low-z contaminants. The main physical driver behind our Pop III colour selections are the (marginally) higher Balmer EWs for Pop III galaxies, together with their lack of (high EW) metal lines, which each contribute a significant 'magnitude excess' in their respective filters.

We find that a combination of NIRCam and MIRI photometry yields the most reliable Pop III colour selection, advocating for the use of the *F444W*−*F560W*, *F560W*−*F770W* colour–colour selection at $z \sim 8$. Assuming 5σ flux density detections, there will likely be some contamination of the Pop III region of the colour–colour plane by both metal-poor ($Z = 0.02$ Z$_\odot$) and metal-rich ($Z =$ Z$_\odot$) galaxies. These systems have comparable Hα EWs (in *F560W*) to Pop III, while also having relatively low EW [O III] λ5007 (in *F444W*) and [S III] $\lambda\lambda$9069, 9531 (in *F770W*) emission lines. This colour selection can be applied at $7.55 < z < 8.10$. However, if $Z =$ $Z_\odot$ galaxies are not considered as a contaminant concern at these redshifts, then the colour selection can be applied over the wider $7.00 < z < 8.35$ redshift interval. Even with perfect photometry (i.e. zero observational errors) however, there will still be contamination by extremely metal-poor galaxies ($Z \leq 0.02\,Z_\odot$). However, with deep follow-up spectroscopy, one will be able to readily distinguish between Pop III galaxies and these non-pristine contaminants.

Given that detections in the MIRI *F770W* filter will be challenging, we also discuss an alternative NIRCam + MIRI colour selection that substitutes the MIRI *F770W* filter for the much more sensitive NIRCam *F410M* (or *F356W*) filter. This colour selection therefore does not require as substantial of a flux boost from gravitational lensing and/or elevated Pop III stellar masses to be applied, but does suffer from contamination by $Z = Z_\odot$ galaxies.

We also introduce two other colour–colour selections, which only require NIRCam photometry, thus needing even shorter integration times to actually apply. These are the [O III] λ5007 versus Lyα selection (i.e. *F410M*−*F444W*, *F115W*−*F150W*), and the [O III] λ5007 versus [O II] selection (i.e. *F410M*−*F444W*, *F277W*−*F335M*). However, these colour selections have their own caveats which likely limit their practical use.

Additionally, we consider the prospects for identifying potential Pop III candidates with slitless spectroscopic emission-line surveys with *JWST*. We focused on three bright, sensitive tracers of Pop III stars: Hβ, Lyα, and He II λ1640. Lyα is intrinsically very bright and so in principle would be readily available with NIRISS, requiring only ∼1 h integrations. However, owing to IGM attenuation/scattering, the observed Lyα flux will be substantially reduced, thereby likely making this line impractical to search for in slitless observations. Instead, Hβ and He II λ1640 seem more promising, though would still require deep-to-ultra-deep observations, at 15–150 and 50–1700 h, respectively. Hence, the flux boost from moderate-to-high lensing ($\mu \sim 5$) and or from observing moderately massive Pop III galaxies ($M_* \sim 5 \times 10^6$ M$_\odot$) will likely again be essential.

Finally, we focus on the additional Pop III constraints that can be derived from follow-up spectroscopy on potential Pop III candidates with NIRSpec. We find that with the NIRSpec/G395M grating, 5σ detections of Hβ can readily be achieved (∼1–10 h) for the Pop III.1 and Pop III.2 IMFs. In principle, a measurement of the Hβ rest-frame EW can be used to distinguish between Pop III and non-Pop III galaxies. However, the difference in EW immediately after a starburst is in fact very small, being only ∼0.1 dex. Furthermore, owing to slight differences in the Hβ EWs predicted by different models, as well as a secondary dependence on covering fraction $f_{\rm cov}$, it may be difficult in practice to make definitive inferences on the Pop III nature of a galaxy from a measurement of the Hβ EW.

Echoing earlier works (see e.g. Schaerer 2002, 2003; Raiter et al. 2010; Grisdale et al. 2021; Nakajima & Maiolino 2022), we find that the He II λ1640 emission line serves as the optimal Pop III indicator. Indeed, a measurement of the He II λ1640 line enables one to both definitively identify Pop III galaxies, as well as place constraints on the Pop III IMF. If both He II λ1640 and Hβ are detected, then there are merits to computing their line ratio, as this is less sensitive to the (perhaps unknown) ionization parameter U. Deep-to-ultra-deep integrations (5–150 h) with NIRSpec/G140M will be needed to detect He II λ1640 at 5σ at $z \sim 8$. With moderate ($\mu = 2$–3) lensing and/or moderately massive (2–3 $\times$ 10^6 M$_\odot$) Pop III galaxies, such line detections can be achieved in medium-sized *JWST* GO programs.

Given the characteristically high He II λ1640 EWs for Pop III galaxies (relative to non-Pop III), we investigate the prospects for identifying Pop III candidates from NIRCam imaging surveys that target this line. As Pop III galaxies still have a relatively low (in an absolute sense) He II λ1640 EW (∼10–100 Å, rest-frame), we find that medium-band imaging will be essential, as even then the photometric signal we are looking for is rather small ($\Delta m = 0.30$ mag, 0.15 mag for the Pop III.1 and Pop III.2 IMFs, respectively). Therefore, owing to NIRCam's greater sensitivity and imaging footprint compared to MIRI, NIRCam medium-band imaging campaigns that search for high EW He II λ1640 emitters may perhaps be a viable alternative to the demandingly deep imaging required with MIRI *F560W* and *F770W*.

Since [O III] λ5007 and Hβ are both simultaneously observable with NIRSpec/G395M at $z = 8$, we looked into the metallicity constraints that can be placed from a 5σ Hβ detection and [O III] λ5007 non-detection. We find that this likely implies a metallicity $Z \leq 0.02\,Z_\odot$. Lowering the upper limit on the metallicity down to $Z \leq Z_\odot/140$ would require an integration time that is 10 $\times$ longer than needed to detect Hβ at 5σ.

Thus, observing and identifying Pop III galaxies with certainty will be a challenging task for *JWST*, likely requiring very deep imaging and spectroscopy to achieve the required S/N for robust detections. All of *JWST*'s key scientific instruments, namely NIRCam, MIRI, NIRISS, and NIRSpec, will likely play a crucial role in our search for the first stars. Indeed, in this ambitious quest, we will likely need to leverage on the flux boost from gravitational lensing and hope for fortuitous imaging of moderate-to-high mass Pop III galaxies. However, it is with the future synergy between space and ground, drawing on the enhanced sensitivity of the next-generation of extremely large telescopes, that we will be able to readily detect the bright He II λ1640 signature of Pop III galaxies.

ACKNOWLEDGEMENTS

We thank the referee for their useful comments which helped to improve this article. JT thanks Rebecca Bowler, Andrew Bunker, Mark Dickinson, Jeyhan Kartaltepe, Harley Katz, and Laura Pen-

tericci for useful discussions which helped improve the quality of this manuscript. JT, CC, and NA acknowledge support by the ERC Advanced Investigator Grant EPOCHS (788113) from the European Research Council (ERC) (PI Conselice). DA and TH acknowledge support from STFC in the form of PhD studentships. RM acknowledges support from the ERC Advanced Grant 695671 'QUENCH'. RM acknowledges support by the Science and Technology Facilities Council (STFC). EZ acknowledges funding from the Swedish National Space Agency. LF acknowledges financial support from Coordenação de Aperfeiçoamento de Pessoal de Nível Superior – Brazil (CAPES) in the form of a PhD studentship.

This work is based on observations made with the NASA/ESA *Hubble Space Telescope* (*HST*) and NASA/ESA/CSA *JWST* obtained from the `Mikulski Archive for Space Telescopes` (`MAST`) at the *Space Telescope Science Institute* (*STScI*), which is operated by the Association of Universities for Research in Astronomy, Inc., under NASA contract NAS 5–03127 for *JWST*, and NAS 5–26555 for *HST*. These observations are associated with *JWST* program 1345.

This research made use of Astropy,[1] a community-developed core PYTHON package for Astronomy (Astropy Collaboration 2013; Price-Whelan et al. 2018).

DATA AVAILABILITY

The Zackrisson et al. (2011) models used in this article are available at: https://www.astro.uu.se/ez/yggdrasil/yggdrasil.html. The Nakajima & Maiolino (2022) models used in this article will be shared on reasonable request to Kimihiko Nakajima. Any remaining data underlying the analysis in this article will be shared on reasonable request to the first author.

REFERENCES

Adams N. J. et al., 2023a, MNRAS, 518, 4755
Adams N. J. et al., 2023b, preprint (arXiv:2304.13721)
Arnouts S., Cristiani S., Moscardini L., Matarrese S., Lucchin F., Fontana A., Giallongo E., 1999, MNRAS, 310, 540
Astropy Collaboration, 2013, A&A, 558, A33
Bagley M. B. et al., 2023b, preprint (arXiv:2302.05466)
Bagley M. B., 2023a, ApJ, 946, 12
Baldwin J. A., Phillips M. M., Terlevich R., 1981, PASP, 93, 5
Bertin E., Arnouts S., 1996, A&AS, 117, 393
Brammer G. B., van Dokkum P. G., Coppi P., 2008, ApJ, 686, 1503
Bromm V., Coppi P. S., Larson R. B., 1999, ApJ, 527, L5
Bromm V., Larson R. B., 2004, ARA&A, 4., 79
Bromm V., Yoshida N., 2011, ARA&A, 49, 373
Bromm V., Yoshida N., Hernquist L., 2003, ApJ, 596, L135
Calzetti D., Armus L., Bohlin R., Kinney A., Koornneef J., Storchi-Bergmann T., 2000, ApJ, 533, 682
Castellano M. et al., 2022, A&A, 662, A115
Chabrier G., Baraffe I., Allard F., Hauschildt P., 2000, ApJ, 542, 464
Curti M. et al., 2022, MNRAS, 512, 4136
Dunlop J. S., 2013, Observing the First Galaxies, 1 edn.. Springer Berlin, Heidelberg
Evans C. et al., 2015, preprint (arXiv:1501.04726)
Ferland G. J. et al., 2013, Rev. Mex. Astron. y Astrofis., 49, 137
Ferland G. J., Korista K. T., Verner D. A., Ferguson J. W., Kingdon J. B., Verner E. M., 1998, PASP, 110, 761
Ferrara A., Pettini M., Shchekinov Y., 2000, MNRAS, 319, 539
Ferreira L. et al., 2022, ApJ, 938, L2
Gardner J. P. et al., 2006, Space Sci. Rev., 123, 485
Grisdale K., Thatte N., Devriendt J., Pereira-Santaella M., Slyz A., Kimm T., Dubois Y., Yi S. K., 2021, MNRAS, 501, 5517
Harikane Y. et al., 2020, ApJ, 896, 93
Hartwig T. et al., 2018, MNRAS, 478, 1795
Hartwig T. et al., 2022, ApJ, 936, 45
Ilbert O. et al., 2006, A&A, 457, 841
Inayoshi K., Li M., Haiman Z., 2018, MNRAS, 479, 4017
Inayoshi K., Onoue M., Sugahara Y., Inoue A. K., Ho L. C., 2022, ApJ, 931, L25
Inoue A. K., 2011, MNRAS, 415, 2920
Inoue A. K., Shimizu I., Iwata I., Tanaka M., 2014, MNRAS, 442, 1805
Johnson J. L., 2013, Formation of the First Galaxies: Theory and Simulations, Springer, Berlin, Heidelberg, p. 177
Johnson J. L., Aykutalp A., 2019, ApJ, 879, 18
Johnson J. L., Greif T. H., Bromm V., 2008, MNRAS, 388, 26
Katz H. et al., 2022, MNRAS, 510, 5603
Katz H., Kimm T., Ellis R. S., Devriendt J., Slyz A., 2023, MNRAS, 524, 351
Kewley L. J., Dopita M. A., Sutherland R. S., Heisler C. A., Trevena J., 2001, ApJ, 556, 121
Kroupa P., 2001, MNRAS, 322, 231
Laporte N. et al., 2019, MNRAS, 487, L81
Laporte N., Meyer R. A., Ellis R. S., Robertson B. E., Chisholm J., Roberts-Borsani G. W., 2021, MNRAS, 505, 3336
Madau P., Ferrara A., Rees M. J., 2001, ApJ, 555, 92
Maiolino R. et al., 2008, A&A, 488, 463
Miralda-Escudé J., 2003, Science, 300, 1904
Moriwaki K. et al., 2018, MNRAS, 481, L84
Nakajima K., Maiolino R., 2022, MNRAS, 513, 5134
Oesch P. A. et al., 2023, preprint (arXiv:2304.02026)
Osterbrock D. E., Ferland G. J., 2006, Astrophysics of gaseous nebulae and active galactic nuclei. University Science Books, Sausalito, CA
Pallottini A., Ferrara A., Gallerani S., Salvadori S., D'Odorico V., 2014, MNRAS, 440, 2498
Planck Collaboration, 2020, A&A, 641
Pontoppidan K. M. et al., 2016, Proc. SPIE, 9910, 991016
Price-Whelan A. M. et al., 2018, AJ, 156, 123
Raiter A., Schaerer D., Fosbury R. A., 2010, A&A, 523, A64
Riaz S., Hartwig T., Latif M. A., 2022, ApJ, 937, L6
Salpeter E. E., 1955, ApJ, 121, 161
Sarmento R., Scannapieco E., Cohen S., 2018, ApJ, 854, 75
Sarmento R., Scannapieco E., Pan L., 2017, ApJ, 834, 23
Schaerer D., 2002, A&A, 382, 28
Schaerer D., 2003, A&A, 397, 527
Schauer A. T. P., Drory N., Bromm V., 2020, ApJ, 904, 145
Shapley A. E. et al., 2015, ApJ, 801, 88
Skidmore W., 2015, Res. Astron. Astrophys., 15, 1945
Stark D. P. et al., 2015, MNRAS, 454, 1393
Stefanon M. et al., 2017, ApJS, 229, 32
Steidel C. C. et al., 2014, ApJ, 795, 165
Stiavelli M., Trenti M., 2010, ApJ, 716, 190
Tan J. C., McKee C. F., 2004, ApJ, 603, 383
Vanzella E. et al., 2023, ApJ, 945, 53
Venditti A., Graziani L., Schneider R., Pentericci L., Di Cesare C., Maio U., Omukai K., 2023, MNRAS, 522, 3809
Vikaeus A., Zackrisson E., Schaerer D., Visbal E., Fransson E., Malhotra S., Rhoads J., Sahlén M., 2022, MNRAS, 512, 3030
Windhorst R. A. et al., 2018, ApJS, 234, 41
Yang S., Lidz A., 2020, MNRAS, 499, 3417
Zackrisson E. et al., 2012, MNRAS, 427, 2212
Zackrisson E., Bergvall N., Olofsson K., Siebert A., 2001, A&A, 375, 814
Zackrisson E., González J., Eriksson S., Asadi S., Safranek-Shrader C., Trenti M., Inoue A. K., 2015, MNRAS, 449, 3057
Zackrisson E., Inoue A. K., Jensen H., 2013, ApJ, 777, 39
Zackrisson E., Rydberg C. E., Schaerer D., Stlin G., Tuli M., 2011, ApJ, 740, 13

[1] http://www.astropy.org

SUPPORTING INFORMATION

Supplementary data are available at *MNRAS* online.

Figure S1. Similar to Fig. 3, but now using the Nakajima & Maiolino (2022) models.
Figure S2. Similar to the [O III]−Hα, Hα−[S III] colour selection in Fig. 3, but now using the analogous redder filters (as the high EW emission lines underpinning the colour selection are redshifted to longer wavelengths) to select Pop III galaxies at $z \sim 10$.
Figure S3. Owing to the challenge in actually detecting Pop III galaxies in the MIRI *F1000W* filter, we advocate for this alternative [O III], [O III]−Hα colour selection (similar to Fig. 4, but now applied at $z \sim 10$), which leverages on the deep *F560W* and *F770W* imaging that will need to be taken to identify $z \sim 8$ Pop III candidates, as well as the much greater NIRCam *F444W* sensitivity (relative to MIRI *F1000W*).
Figure S4. Similar to the [O III], Lyα colour selection in Fig. 5, but now using the analogous redder filters to select Pop III galaxies at $z \sim 10$.
Figure S5. Similar to the [O III], [O II] colour selection in Fig. 6, but now using the analogous redder filters to select Pop III galaxies at $z \sim 10$.
Table S1. Similar to Table 1, but now for Pop III galaxies at $z = 10$.
Table S2. Similar to Table 3, but now for Pop III galaxies at $z = 10$.
Table S3. Similar to Table 4, but now for Pop III galaxies at $z = 10$.

Please note: Oxford University Press is not responsible for the content or functionality of any supporting materials supplied by the authors. Any queries (other than missing material) should be directed to the corresponding author for the article.

This paper has been typeset from a TEX/LATEX file prepared by the author.